



Gap Analysis for Integrated Atmospheric ECV Climate Monitoring (GAIA-CLIM)

Work package number	WP4
Work package title	Assessment of reference data in global assimilation systems and characterisation of key satellite datasets
Task number	T4.1
Task title	Assessment of new satellite missions
Deliverable report title	Calibration/validation study of AMSR2 on GCOM-W1
Document version	1.1 (22 January 2015)



Met Office

Stuart Newman

Bill Bell



Kirsti Salonen



This project has received funding from the European Union's Horizon 2020 research and innovation programme under grant agreement No 640276

Author affiliations

Stuart Newman and Bill Bell
Met Office
FitzRoy Road
Exeter
EX1 3SP
United Kingdom

Kirsti Salonen
European Centre for Medium-Range Weather Forecasts
Shinfield Park
Reading
RG2 9AX
United Kingdom

Contents

1. Introduction	2
2. Data description and data analysis methodology	3
2.1. AMSR2 instrument description.....	4
2.2. Met Office archived data	5
2.3. ECMWF archived data.....	6
2.4. Data selection	7
3. Results	12
3.1. Monthly mean O-B climatology	12
3.2. Monthly distributions of O-B	17
3.3. Geographically localised anomalies	21
3.4. Dependence on atmospheric transmittance	22
3.5. Dependence on orbital angle	25
3.6. Comparison of ascending and descending nodes	29
3.7. Dependence on scan position.....	30
3.8. Dependence on sea surface temperature	33
3.9. Daily statistics (seasonal variability)	34
4. Preliminary conclusions	37
5. Acknowledgements.....	38
6. References.....	39
7. Appendix: monthly O-B climatology maps.....	41

1. Introduction

The exploitation of geophysical information from Earth Observation (EO) space borne instruments depends critically on the calibration and validation of these data to a recognised standard. To date, validation of satellite instruments and derived products has been ad hoc, for example relying on satellite-to-satellite intercomparisons which lack fully traceable estimates of radiometric uncertainty. Activities within the GAIA-CLIM consortium aim to build an improved capability for satellite calibration/validation (cal/val), ultimately leading to a database of reference quality data for robust characterisation of satellite measurement uncertainties.

The framework of Numerical Weather Prediction (NWP) is attractive for assessment of satellite instrument performance, since these models ingest large volumes of observational data daily and offer comprehensive spatial and temporal sampling. Modern data assimilation (DA) systems blend information from observations and the forecast model to arrive at an optimal estimate (analysis) of the atmospheric state. Model physics constraints ensure that the resulting global atmospheric fields are physically consistent. NWP forecasts are routinely validated by comparison with reference observations (usually radiosondes) or comparator NWP analyses, and accurate representations of three-dimensional temperature and humidity fields make NWP systems effective in detecting subtle artefacts in satellite data (e.g. Lu and Bell, 2014).

NWP model data are not yet traceable to an absolute calibration standard. Activities within GAIA-CLIM Work Package 4 aim to develop the necessary infrastructure for the routine monitoring of reference networks such as the GCOS Reference Upper Air Network (GRUAN), linking NWP to SI standards. This report considers the potential for NWP to perform a cal/val study for a new satellite mission (AMSR2 on the GCOM-W1 platform). We focus on characterising the spatial variability, geophysical state dependence and instrument state dependence of biases (in observation space) using DA systems employed operationally by two independent forecasting centres (ECMWF and the Met Office). In this way the physical mechanisms underlying the observed biases can be investigated.

2. Data description and data analysis methodology

It is modern practice at NWP centres to assimilate satellite radiances (sometimes termed Level 1 data), in preference to products retrieved from the radiances such as temperature and humidity profiles (Level 2 data). A fast radiative transfer model is required to map between radiances in the spectral domain and Earth system variables, for which the Met Office and ECMWF use RTTOV (Saunders et al., 1999). In vector notation, we represent the atmosphere and surface variables on which the radiances depend as a state vector \mathbf{x} and compute the simulated satellite radiance $H(\mathbf{x})$ for RTTOV observation operator H .

ECMWF and the Met Office have implemented a four-dimensional NWP data assimilation system (4D-Var), see e.g. Rabier et al. (2000), Rawlins et al. (2007). The Met Office also employs a simplified 1D-Var pre-processing step. The 1D-Var assimilation, which is analogous to that performed within the full 4D-Var system, proceeds by minimising a cost function,

$$J(\mathbf{x}) = \frac{1}{2}(\mathbf{x}-\mathbf{x}_b)^T \mathbf{B}^{-1}(\mathbf{x}-\mathbf{x}_b) + \frac{1}{2}(\mathbf{y}-H(\mathbf{x}))^T \mathbf{R}^{-1}(\mathbf{y}-H(\mathbf{x})), \quad (1)$$

in order to estimate the most probable solution for the state vector \mathbf{x} . Here, \mathbf{x}_b is the a priori background vector from the NWP forecast model, \mathbf{y} is the set of measurements (radiance for satellite channels of interest), \mathbf{B} and \mathbf{R} represent the error covariance characteristics of the background state and observations respectively, and $H(\mathbf{x})$ is the set of simulated radiances.

Examples of observations and equivalent simulated brightness temperatures are shown for a single channel of AMSR2 in Figure 1. It can be seen that global variations in observed brightness temperature are well reproduced in the RTTOV simulations, due to accurate representations of variables such as temperature and humidity profiles in the NWP fields.

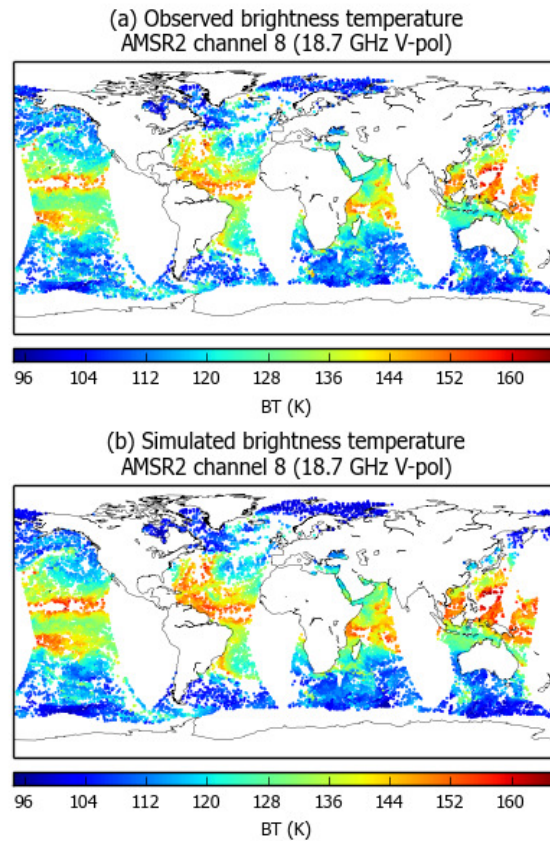


Figure 1. (a) AMSR2 channel 8 brightness temperature as ingested into the Met Office 1D-Var assimilation (observations shown without bias correction). Data are plotted for the period spanning 31 October 2014 2100 UTC to 2 November 2014 0300 UTC. (b) Brightness temperatures simulated from NWP fields using RTTOV for observation locations as in (a).

The difference between the observations and model background simulation, $y-H(\mathbf{x}_b)$, is variously termed the innovation, first guess departure or simply O-B for observed minus background difference. This is the key parameter we use as a diagnostic in this report. We examine how these departures vary spatially and seek to determine their dependence on geophysical variables and AMSR2 instrument state.

2.1. AMSR2 instrument description

The Advanced Microwave Scanning Radiometer 2 (AMSR2) was launched on the Japan Aerospace Exploration Agency (JAXA) GCOM-W1 spacecraft on 18 May 2012. It is a conically-scanning passive microwave radiometer with fourteen channels (seven frequencies with dual polarisation between 6.7 GHz and 89 GHz as shown in Table 1).

Table 1. Characteristics of AMSR2 channels. Source: Imaoka et al. (2010).

Band (GHz)	Polarisation	Footprint size (km × km)
6.93	V, H	62 × 35
7.3	V, H	62 × 35
10.65	V, H	42 × 24
18.7	V, H	22 × 14
23.8	V, H	19 × 11
36.5	V, H	12 × 7
89.0	V, H	5 × 3

AMSR2 is a follow-on mission from previous JAXA instruments AMSR and AMSR-E. Several major changes have been made to improve the AMSR2 design (Imaoka et al., 2010). These include a larger main reflector, thermal design changes to address temperature non-uniformities, and extensive sunlight shielding. A hot load calibration target and cold sky mirror are used for two-point radiometric calibration. The 2 m diameter main reflector rotates at 40 revolutions per minute providing Earth views with a fixed incidence angle of 55 degrees.

Level 2 products are generated from AMSR2 radiances using algorithms maintained by JAXA¹, NASA² and Remote Sensing Systems³. These include sea surface temperature, surface wind speed, integrated water vapour, cloud liquid water, precipitation rate, sea ice concentration, snow depth and soil moisture.

2.2. Met Office archived data

AMSR2 is not yet assimilated operationally at the Met Office, having been tested in global NWP trials during 2015. Concurrently, variational bias correction (VarBC, see Auligné et al., 2007) of raw satellite radiances was also tested, to replace the previous static bias correction scheme. Bias correction is a necessary step in NWP data assimilation systems, since a sub-optimal analysis of the atmospheric state results from using biased observations. Note, however, that the statistics presented in this report are based on the raw observation brightness temperatures for the purposes of instrument cal/val.

¹ http://suzaku.eorc.jaxa.jp/GCOM_W/data/data_w_index.html

² <https://earthdata.nasa.gov/earth-observation-data/near-real-time/download-nrt-data/amsr2-nrt>

³ <http://www.remss.com/missions/amsre>

Since operational data were not available, a rapid cycling suite was set up to perform the following steps at six-hourly intervals:

1. Retrieve AMSR2 observations from the local data store.
2. Retrieve archived NWP fields and auxiliary data for the appropriate 6-hour cycle.
3. Process AMSR2 data in the Observations Processing System (OPS), which includes quality control checks, spatial thinning and 1D-Var retrieval.
4. Pass the accepted observations to 4D-Var (VAR); for this work it was sufficient to run VAR at “outer loop” lower resolution N108 in order to generate updated VarBC coefficients.
5. Write out AMSR2 observations and collocated NWP fields in netCDF format.
6. Use the revised bias correction coefficients in the next cycle.

The NWP fields are independent of the AMSR2 data in this case. Within OPS, the AMSR2 data were screened to remove observations significantly affected by cloud (since in VAR the clear sky version of RTTOV is used). This was achieved by retrieving the liquid water path (LWP) for each observation and rejecting any with a retrieved LWP greater than 0.04 kg/m^2 .

A common data period was agreed between the Met Office and ECMWF, to begin on 1 March 2015 and run for up to 12 months. This provides data over one annual cycle for investigations of temporal trends. Only observations over ocean are considered here.

2.3. ECMWF archived data

AMSR2 observations have been used operationally in the ECMWF system since 12 August 2015. Results from the quality and impact assessment in the ECMWF system using the all-sky radiance assimilation are discussed in Kazumori et al (2015). The AMSR2 radiance data quality was found to be comparable to other microwave imagers (SSMIS and TMI) and the use of AMSR2 in the assimilation generally improves the humidity, temperature and wind first-guess fields in the troposphere with improvements for longer range forecasts as well.

For this study the statistics are calculated from a research experiment where AMSR2 is passively monitored, i.e. the bias correction is updated but the AMSR2 data is not used in the analysis. The experiment uses ECMWF integrated forecasting (IFS) cycle 41r1

with 12-hour 4D-Var, horizontal resolution of T1279 and 137 vertical levels. The experiment configuration is identical to the operational configuration except for the use of a fixed blacklist from February 2015. The data period, in common with the Met Office, was 1 March 2015 onwards.

Some details of the ECMWF data usage differ from those of the Met Office. Microwave observations at ECMWF are processed using an all-sky scheme which allows cloud-affected as well as clear sky observations to be assimilated (Geer et al., 2014). The scattering version of RTTOV is used for the radiative transfer calculations. In addition, the AMSR2 data are spatially averaged (“superobbed”) so that each assimilated observation is the mean of 50 satellite footprints.

2.4. Data selection

We wish to analyse O-B statistics, $\mathbf{y} - H(\mathbf{x}_b)$, such that the simulated radiances $H(\mathbf{x}_b)$ are as reliable a reference as possible. Therefore, we should select cases where the NWP model background state \mathbf{x}_b exhibits small errors and the radiative transfer model H is capable of accurately representing that model state in radiance space. There are some meteorological regimes that are problematic in this regard, such as the presence of clouds for which the NWP forecast model may be in error spatially and temporally, and for which the radiative transfer is complicated. By contrast, in clear skies we expect the NWP model state of temperature and (to a lesser extent) humidity to be accurate for short forecast lead times, and the radiative transfer to be simpler.

At ECMWF cloudy microwave observations are assimilated successfully by representing the observation error as a function of cloud amount (Geer and Bauer, 2011). In this scheme, an effective cloud amount is derived by calculating the normalised polarisation difference at 37 GHz (Petty and Katsaros, 1990; Petty 1994):

$$P_{37} = (T_v - T_h) / (T_{v_clear} - T_{h_clear}). \quad (2)$$

T_v and T_h are respectively the vertically and horizontally polarised 37 GHz brightness temperatures in all sky conditions, while T_{v_clear} and T_{h_clear} are the brightness temperatures for the same observation locations but without the contributions due to clouds or precipitation. At 37 GHz the sea is highly polarised, while contributions due to atmospheric opacity tend to be unpolarised. Thus, P_{37} varies between 1 in clear sky

conditions and 0 in conditions of totally opaque cloud. We can then define an effective cloud amount as

$$C_{37} = 1 - P_{37} \quad (3)$$

where increasing $C_{37} > 0$ indicates increasing amounts of cloud. The cloud amount for observations, C_{37}^o , is computed using observed 37 GHz brightness temperatures as T_v , T_h in Eqn. (2). Similarly, the background cloud amount, C_{37}^b , is computed using *simulated cloudy* 37 GHz brightness temperatures as T_v , T_h , which requires the use of the scattering version of the radiative transfer code RTTOV-SCATT. For both C_{37}^o and C_{37}^b , T_{v_clear} and T_{h_clear} are clear sky simulations.

Figure 2 shows example data for the effective cloud amounts computed by ECMWF and the Met Office. Synoptic scale features giving rise to cloud are clearly visible, and consistent between the two centres. Negative values of C_{37}^o can occur for situations where the model humidity is higher than in reality (Geer and Bauer, 2011).

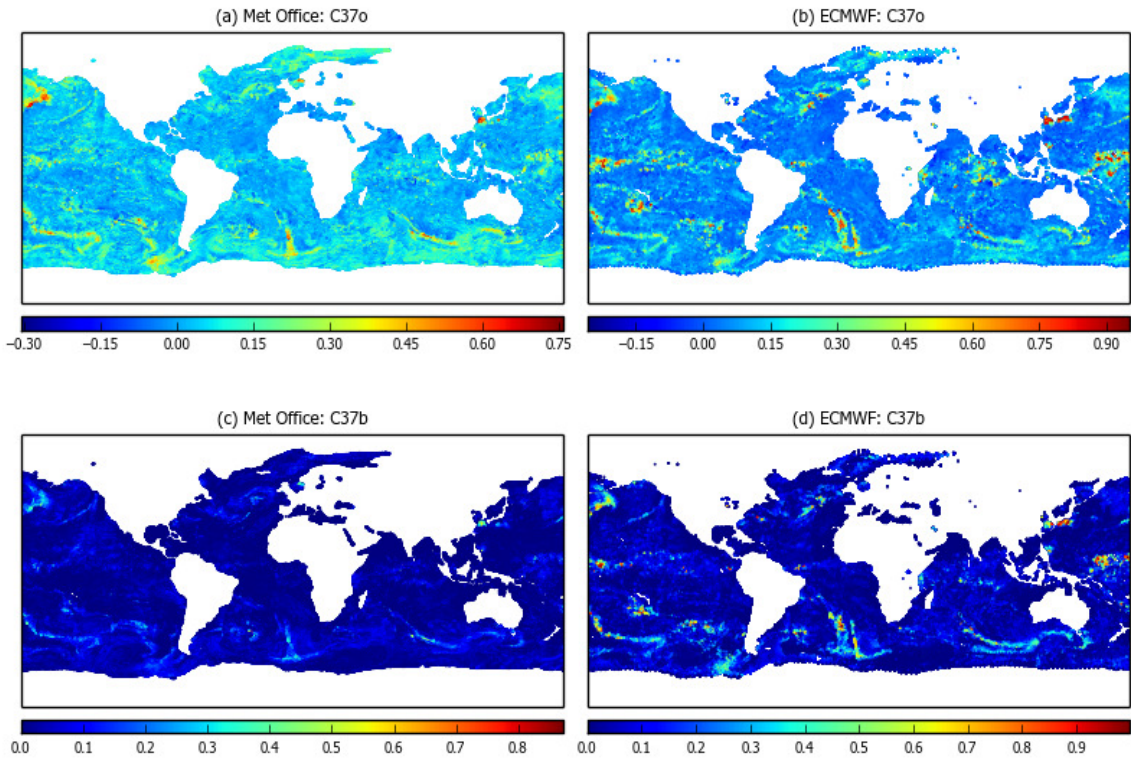


Figure 2. Plots showing effective cloud amounts as described in the text. (a) Met Office C_{37}^o , (b) ECMWF C_{37}^o , (c) Met Office C_{37}^b , (d) ECMWF C_{37}^b . Data have been aggregated for the period 1-9 May 2015.

We can establish the relationship between standard deviation in O-B and cloud amounts, with smallest standard deviations observed for $C_{37}^o \sim 0$, $C_{37}^b \sim 0$. The following empirical criteria were used to exclude cloud-affected data, mandating that:

$$|C_{37}^o| < C_{\text{crit}} \quad (4a)$$

$$|C_{37}^b| < C_{\text{crit}} \quad (4b)$$

$$|C_{37}^o| + |C_{37}^b| < C_{\text{crit}} \quad (4c)$$

A value $C_{\text{crit}} = 0.02$ has been used in this work, chosen empirically as a balance between excluding cloud-affected observations but retaining sufficient numbers for a statistically significant sample.

It was found by inspection that some of the largest O-B outliers (most positive or most negative) were to be found very close to coastlines, particularly for the lower frequency AMSR2 channels which have larger field of view footprints on the ground. Therefore a proximity test was implemented to exclude all satellite fields of view centred within 75 km of any coastline.

It is also apparent from analysing the data that the O-B statistics have a dependency on other parameters. For example, Figure 3 shows how the departures vary with surface temperature. There are clearly larger deviations from the mean for the lowest surface temperatures for both Met Office and ECMWF data. This can partly be explained due to observations at high latitudes where the model sea ice extent may be uncertain and surface emissivity less well known. All data with surface temperatures below 275 K have been removed from the data sets to avoid including these difficult scenes.

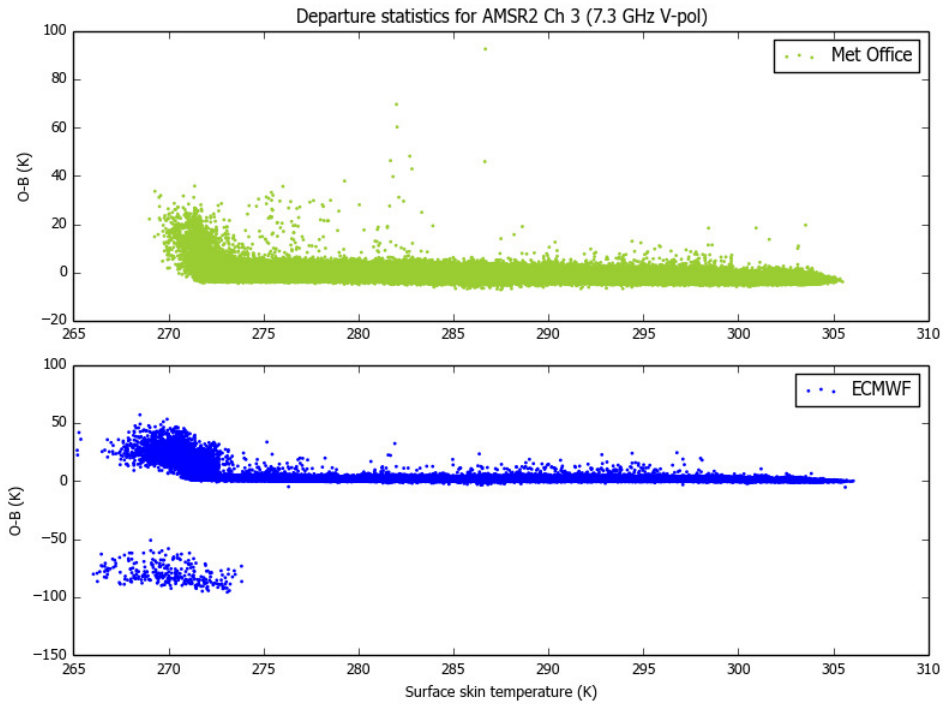


Figure 3. Scatter plots of AMSR2 channel 3 O-B statistics as a function of surface skin temperature, presented for Met Office data (upper panel) and ECMWF data (lower panel). Results shown are all valid data for May 2015.

Another regime that presents difficulties is that of high surface wind speed. Figure 4 compares mean one-month maps of 10m wind speed and AMSR2 channel 5 O-B for both Met Office and ECMWF data sets. In this and other similar plots in this report the data have been aggregated and mean values calculated in 1° longitude by 1° latitude grid boxes. There appears to be a clear correlation between high wind speed and larger O-B values, particularly in the Southern Ocean.

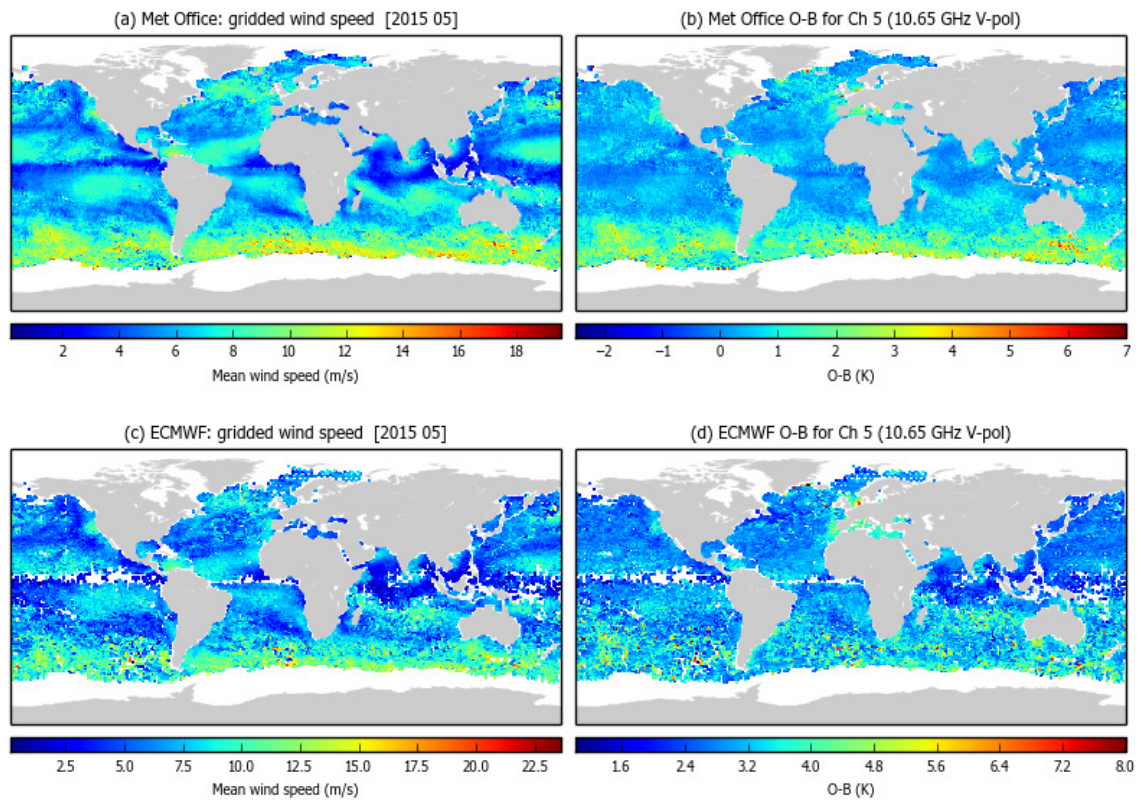


Figure 4. (a) Met Office surface (10 m) wind speed, (b) Met Office AMSR2 channel 5 O-B for the month of May 2015. Data have been aggregated and mean values calculated within 1° longitude \times 1° latitude grid boxes; (c), (d) are as for (a), (b) presenting ECMWF data for the same period. Areas with insufficient number of observations to grid are shown in white.

The same data are presented in a different way in Figure 5. Scatter plots of AMSR2 channel 5 O-B show a clear dependence on surface wind speed, with large positive O-B values for high winds. This behaviour is observed for all the V-polarisation channels; the H-polarisation channels, such as channel 6 in Figure 5, seem to exhibit a somewhat smaller wind speed dependence. In order to consider only the most reliable set of departures, all data with wind speeds exceeding 7 m/s have been excluded for the analysis presented in Section 3.

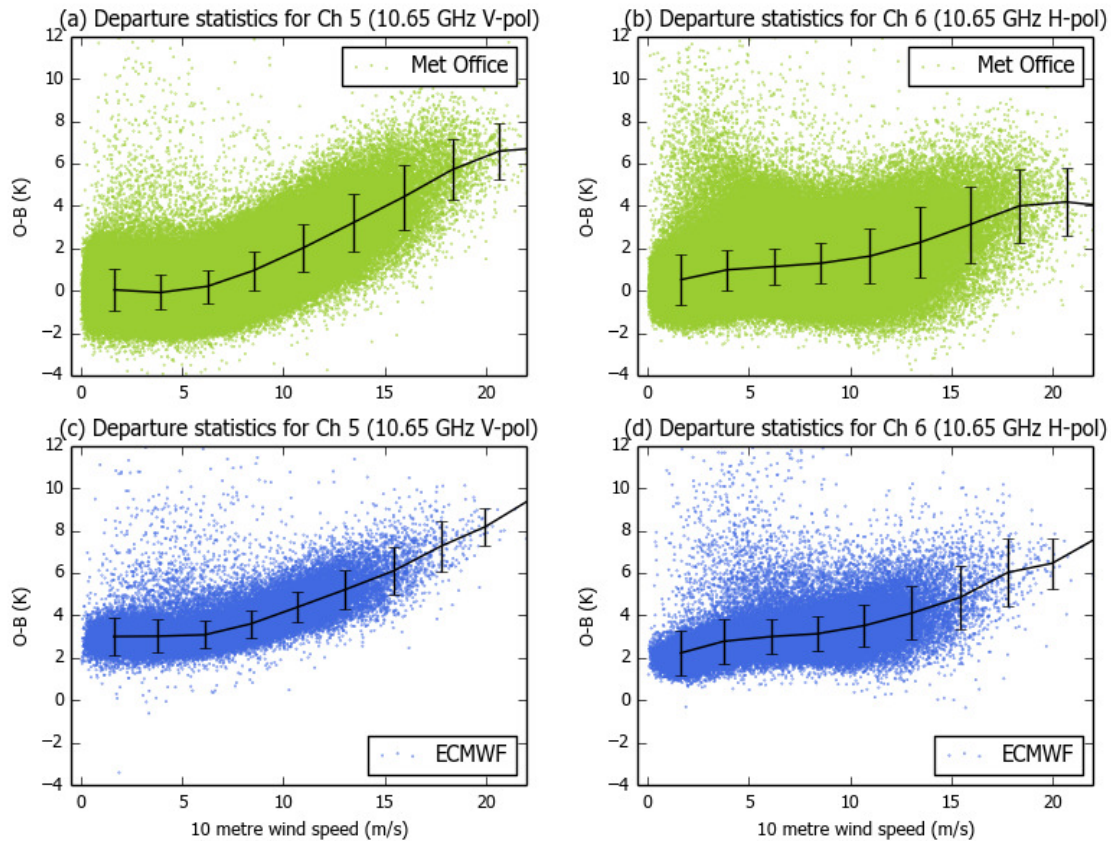


Figure 5. (a) Met Office O-B departure statistics for AMSR2 channel 5 plotted as a function of 10 m wind speed. Each data point is shown as a coloured marker, overlaid with binned data shown in black with error bars. (b) As for (a), showing AMSR2 channel 6 data. (c), (d) As for (a), (b), showing ECMWF data for AMSR2 channels 5 and 6.

3. Results

The effect of filtering the data sets to exclude the fields of view (FOVs) most affected by coastlines, cloudiness and high winds is to reduce the number of observations to analyse. Typical data volumes remaining are in excess of 400,000 Met Office FOVs and 40,000 ECMWF FOVs (from the superobbed set) per month. The resulting data subset is analysed in this section to explore further the dependencies of the departures on instrument, atmospheric and surface variables.

3.1. Monthly mean O-B climatology

Spatial maps of monthly mean climatologies of O-B usefully summarise the geophysical characteristics of the departures. These are presented for the full set of 14 AMSR2 channels in Figure 6, Figure 7, Figure 8 and Figure 9 for an example month (May 2015). Some features are immediately apparent:

1. There is a latitudinal dependence to the O-Bs for several channels. This is particularly apparent for AMSR2 channels 1 and 3 in the Met Office plots and the higher frequency channels for both NWP centres.
2. There are anomalously large O-Bs for certain geographic areas. These include the Mediterranean region for the 10.65 GHz channels and the coastal areas of North America at 18.7 GHz.

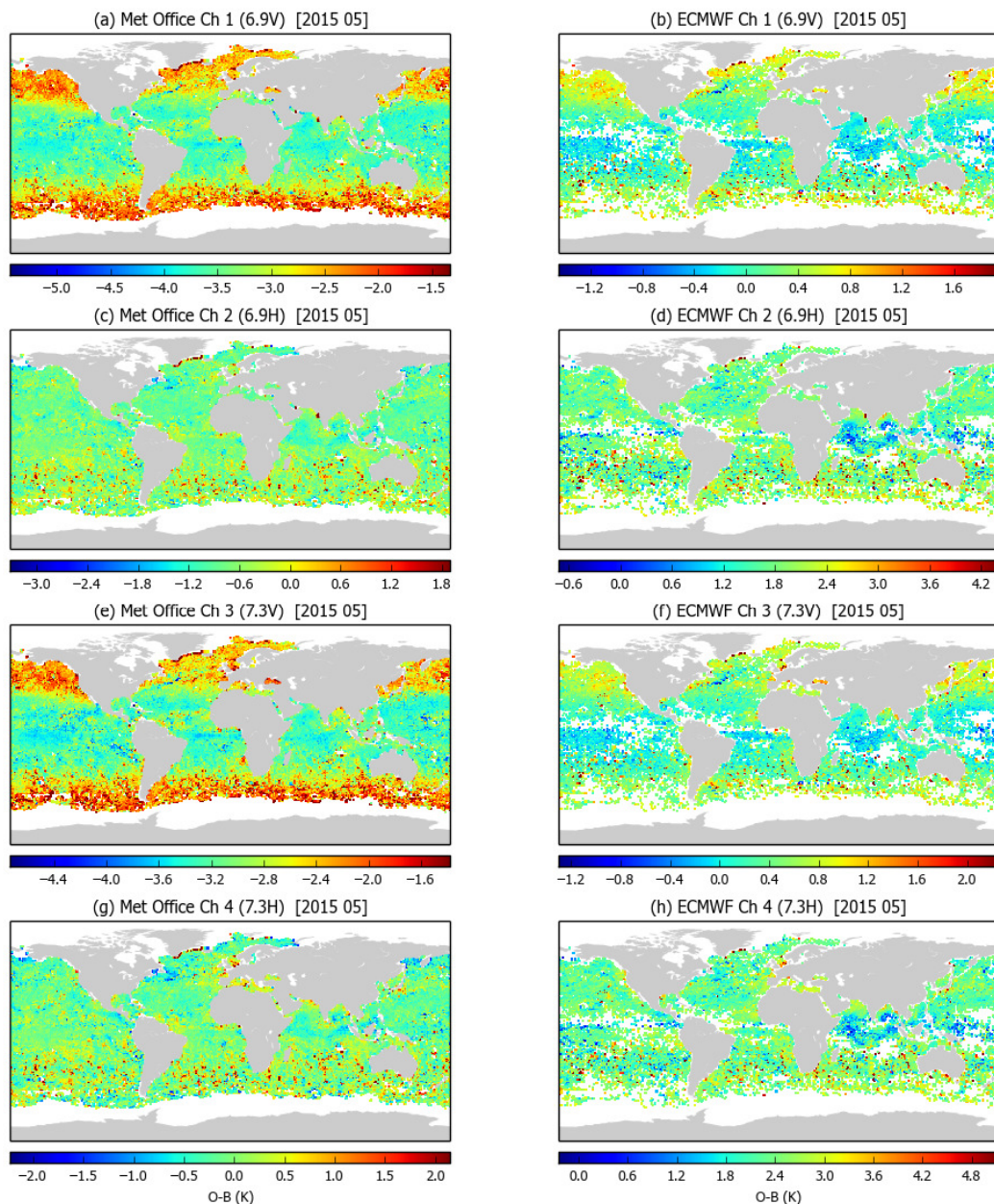


Figure 6. Gridded O-B climatology for May 2015. Met Office departures for AMSR2 channels 1-4 are shown in (a), (c), (e), (g) respectively. ECMWF departures are shown in (b), (d), (f), (h) respectively. The colour scale for each channel is centred at the mean O-B value, with difference between scale minima and maxima set to four times the data standard deviation.

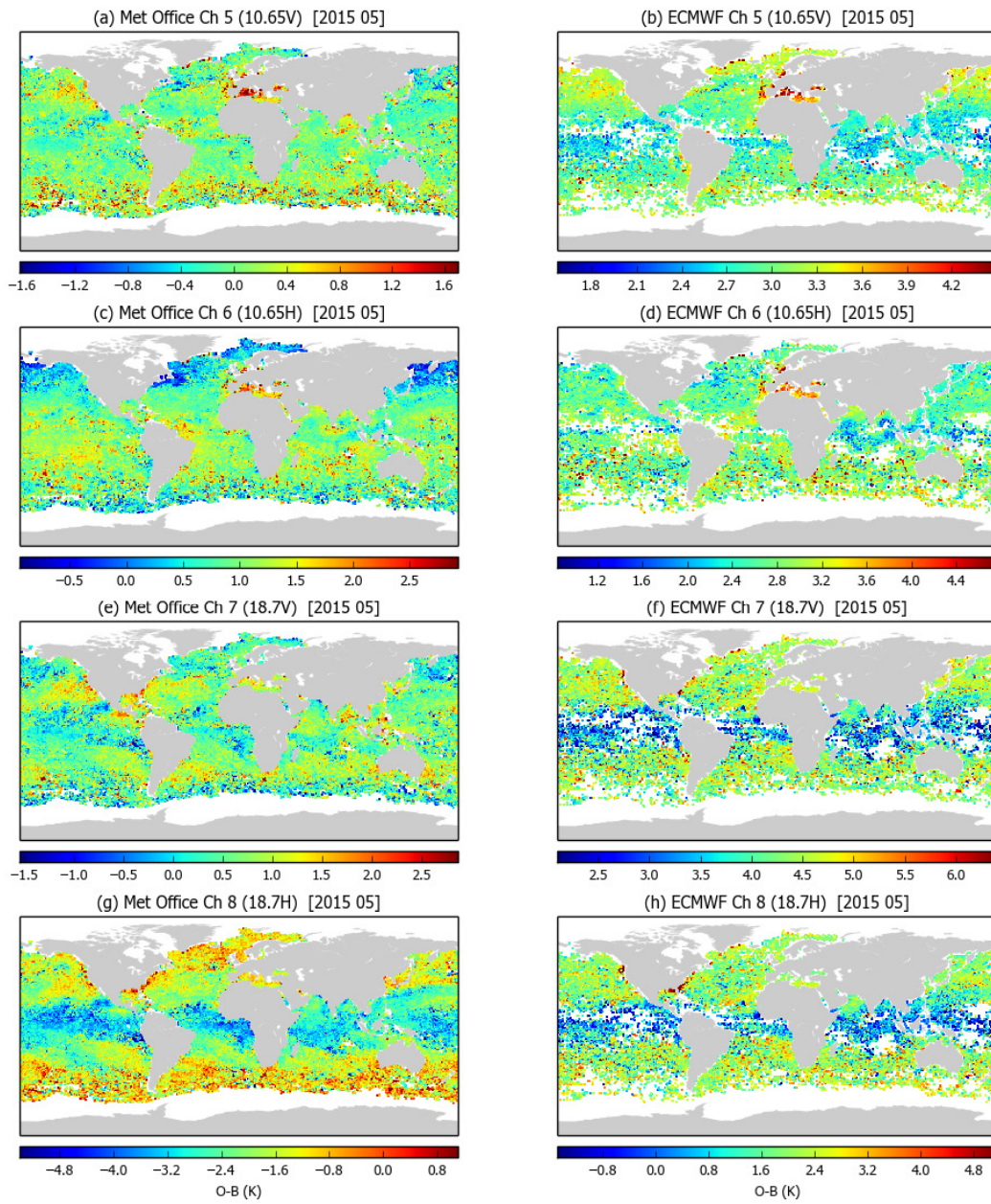


Figure 7. As Figure 6, presenting O-B climatology for AMSR2 channels 5-8.

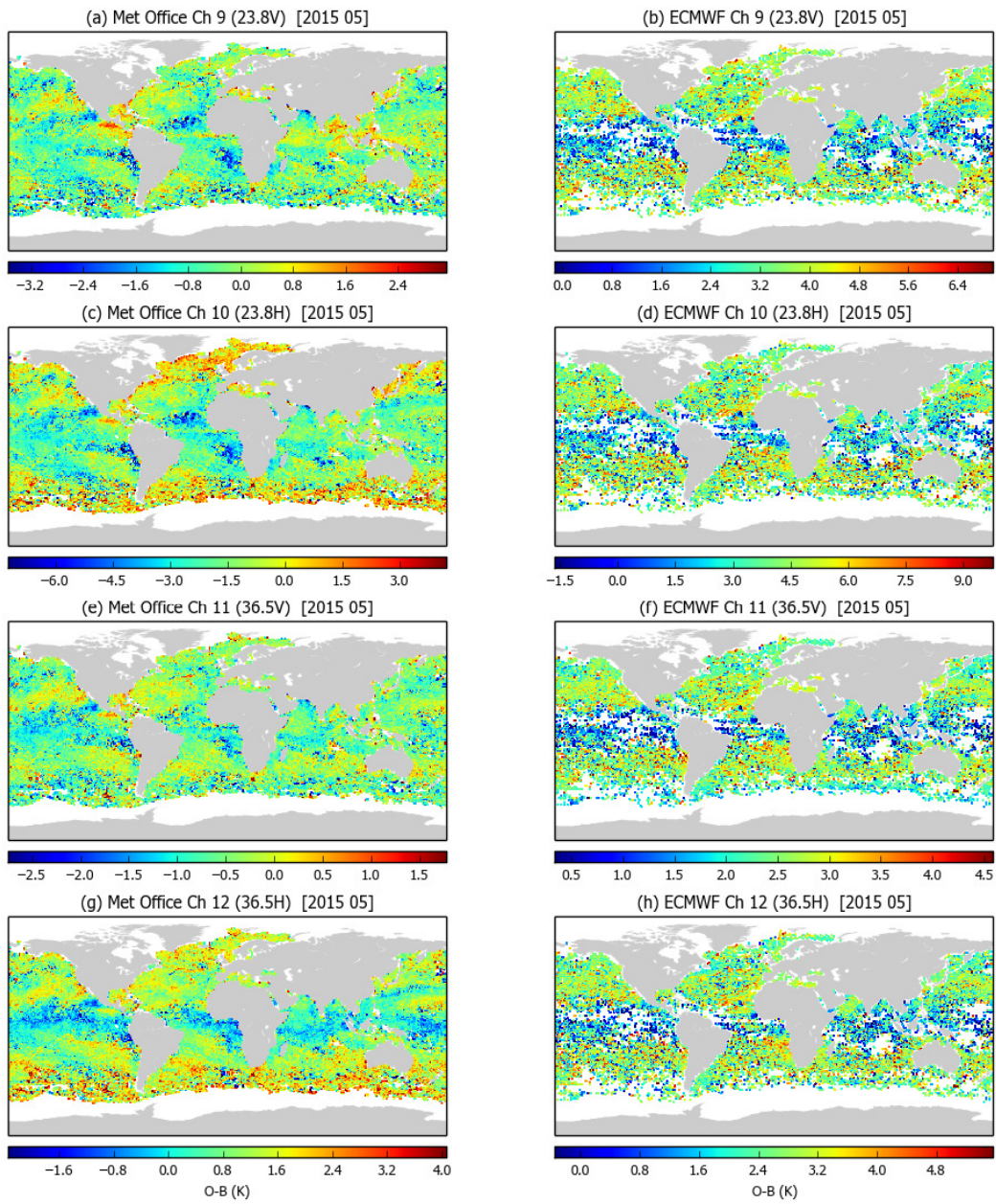


Figure 8. As Figure 6, presenting O-B climatology for AMSR2 channels 9-12.

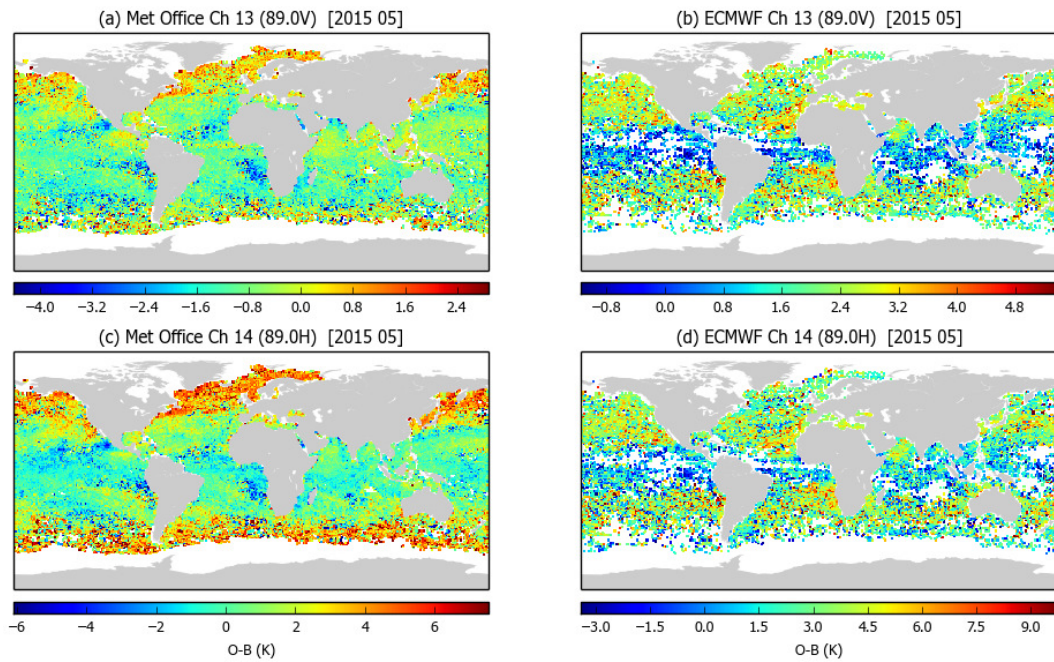


Figure 9. As Figure 6, presenting O-B climatology for AMSR2 channels 13 and 14.

It is unwieldy to present the O-B climatology maps for all channels and all months in this section. Therefore, these are presented at the end of the report (Appendix). The climatology maps are seen to be very stable month by month.

There are a number of candidate explanations for the spatial dependence of O-Bs. These include:

- Radio Frequency Interference (RFI). This is the contamination of satellite-received radiances by external (artificial) sources of electromagnetic radiation. RFI contaminated AMSR2 observations in 18.7 GHz channels in coastal areas of North America were noted by Kazumori et al. (2015).
- Dependence of O-Bs on surface-to-space transmittance. For microwave imager channels the main contribution to (clear sky) opacity is water vapour. In the Tropics the transmittance is reduced relative to higher latitudes due to high total column water vapour (TCWV), which means the satellite radiances are influenced more by the atmospheric humidity and less by the surface emission.
- Orbital variations. The GCOM-W1 spacecraft experiences changes in received solar radiation as it orbits the Earth. In some circumstances these may cause instrument thermal instabilities and affect the radiance calibration.
- Scan dependence of O-Bs. AMSR2 receives radiation from 243 unique scan positions during the conical scan.

- Dependence of O-Bs on sea surface temperature (SST). Together with surface wind speed, the SST is used to predict the ocean emissivity at each AMSR2 frequency.

The following sections explore these issues further.

3.2. Monthly distributions of O-B

An alternative way to present the monthly statistics is to generate probability distribution function (PDF) histograms of the departures. These are shown in Figure 10 for May 2015. It is most striking that the mean O-Bs per channel differ markedly between the Met Office and ECMWF data sets. The spread in distributions for each channel tends to be comparable, but slightly narrower, for ECMWF cf. Met Office data.

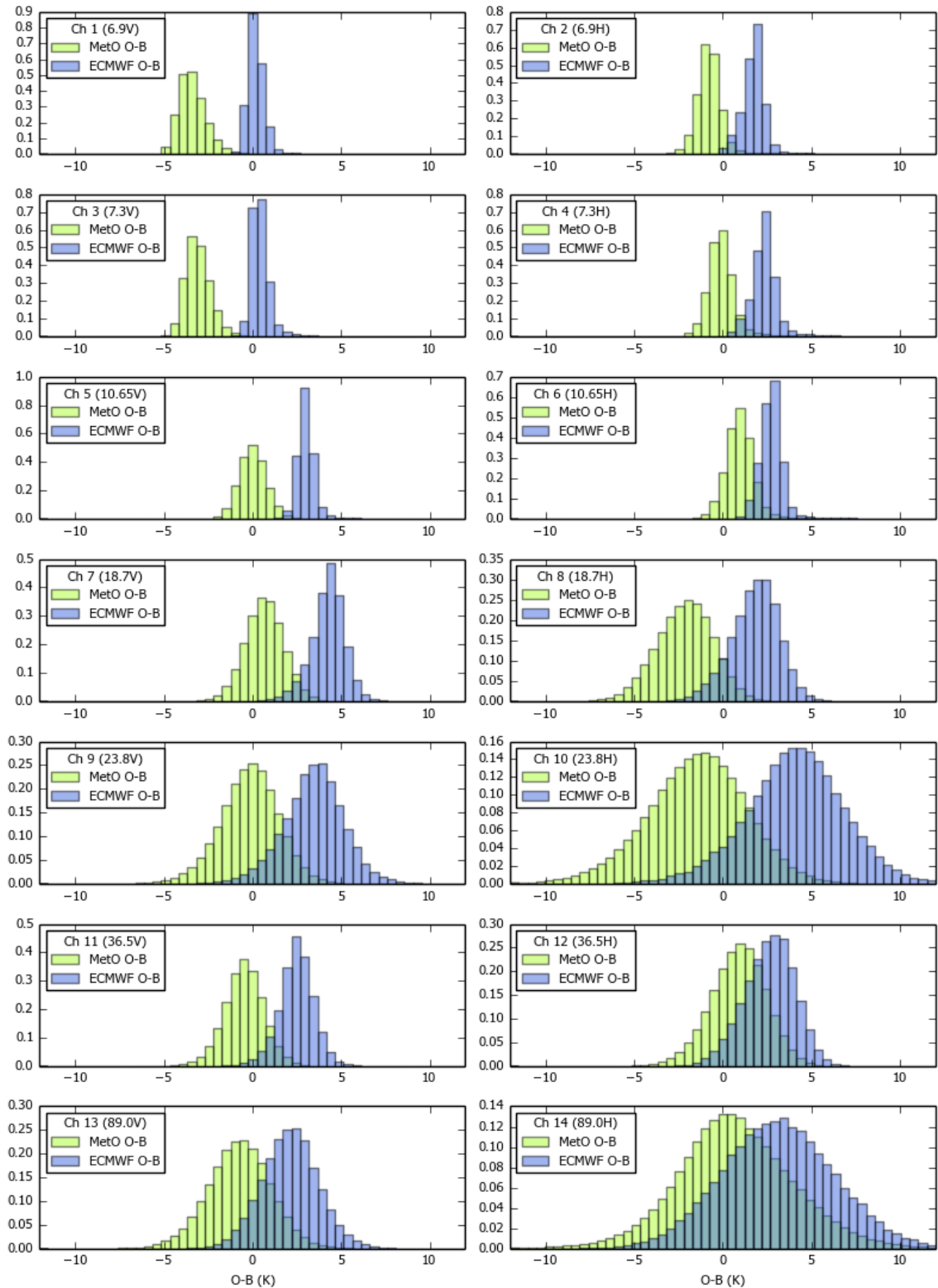


Figure 10. Normalised O-B distributions for the set of 14 AMSR2 channels (see legend) for Met Office ('MetO') and ECMWF data sets. Data are shown for May 2015.

One key difference between the Met Office and ECMWF operational radiative transfer is the assumed formulation for ocean emissivity. At the Met Office, RTTOV is interfaced to

version 3 of the Fast microwave Emissivity Model, FASTEM-3 (Liu and Weng, 2003) for AMSR2 processing. By contrast, ECMWF use a more recently updated version of the model, FASTEM-6 (Kazumori and English, 2015). A notable feature of FASTEM-6 is that it incorporates a newly derived dependence on relative wind direction.

An example of how the FASTEM versions differ is shown in Figure 11 for AMSR2 channel 7. The emissivity is lower for warm Tropical oceans than colder seas at high latitudes in both models, see Figure 11 (c), but FASTEM-3 emissivities are systematically higher than those for FASTEM-6. The surface-emitted radiation can be calculated simply at microwave frequencies as the product of surface temperature and emissivity terms, as presented in Figure 11 (d). (The actual radiation received by the satellite instrument is modulated by the atmospheric transmittance and reflected downwelling radiation.) The Met Office modelled surface emission is consistently higher than ECMWF by around 3-7 K. Since the two centres' sea surface temperature fields do not differ systematically, this is due almost entirely to the emissivity differences. The AMSR2 channel 7 O-B distributions shown in Figure 10 have mean values of 0.66 K (Met Office) and 4.25 K (ECMWF). Given a high surface-to-space transmittance, the mean O-B difference (3.6 K) is directly attributable to the FASTEM differences.

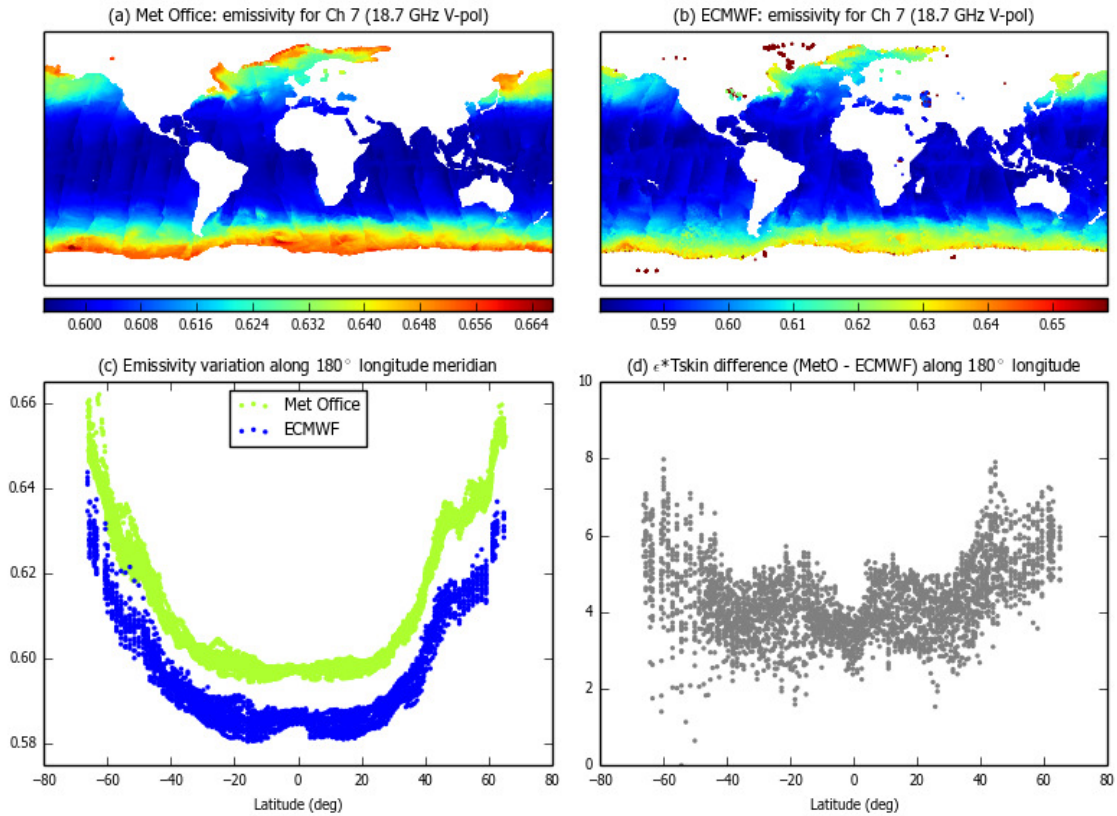


Figure 11. Comparison of AMSR2 channel 7 emissivity modelled by (a) Met Office (FASTEM-3) and (b) ECMWF (FASTEM-6) operational processing. Data have been aggregated for the period 1-9 May 2015. (c) Variation of emissivity as a function of latitude within 1° of the 180° longitude meridian, shown for the Met Office (green) and ECMWF (blue). (d) Difference (Met Office minus ECMWF) in surface-emitted radiation defined as the product of emissivity and surface temperature.

For some AMSR2 channels, such as 1 and 3, the ECMWF O-B PDF is centred closer to 0 K. For other channels, such as 7 and 9, the opposite is true. This analysis exposes the need for reducing the uncertainty in microwave ocean emissivity models, since the emissivity is fundamental for modelling the received top-of-atmosphere radiance for a microwave imager. For channels with greater atmospheric opacity, such as those on microwave temperature and humidity sounders, the surface emissivity plays a more minor role since the dominant source of radiation is due to atmospheric emission. Essential climate variables (ECVs) derived from AMSR2 data, such as SST or TCWV, are subject to uncertainties propagated by an imperfect knowledge of the ocean emission.

3.3. Geographically localised anomalies

O-B climatologies (e.g. Figure 7) show instances of large positive departures for some locations. A detailed example is shown in Figure 12, considering the Central America and Gulf of Mexico area on 1 May 2015. For context, these data include those otherwise excluded by the cloud amount thresholds: it can be seen that clouds are identified in the C_{37}^0 field over Cuba, giving rise to large O-Bs for channels such as 11 and 12. However, other large departures do not seem to be correlated with the cloud field, such as those observed for channels 7 and 8 off the west coast of Florida. High resolution satellite imagery (not shown) indicates this area was free of cloud.

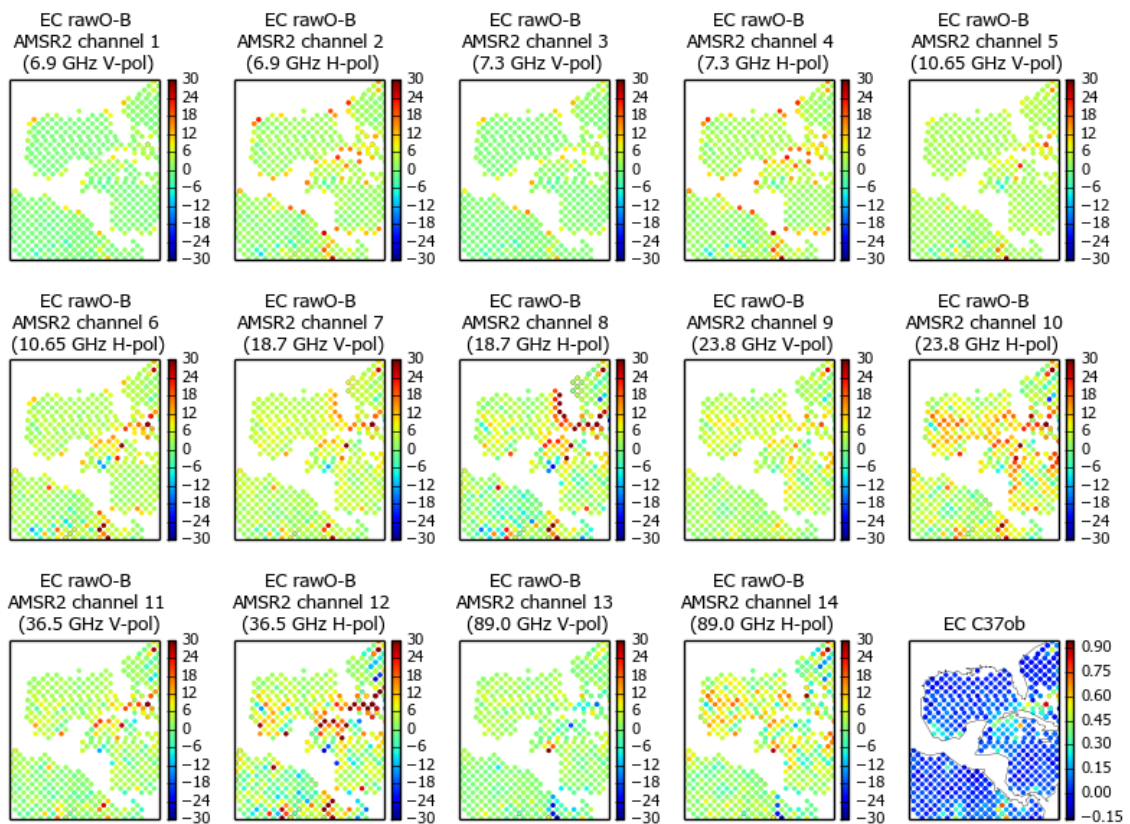


Figure 12. Example plots of AMSR2 O-B values for 24 hours of ECMWF data on 1 May 2015 (first fourteen plots corresponding to AMSR2 channels 1-14, as labelled). The fifteenth plot shows the effective cloud amount C_{37}^0 .

AMSR2 channel 8 O-Bs exceed 30 K for the affected area, as do those for the Met Office data. The most likely cause is RFI which is known to contaminate passive microwave measurements. This was a transient feature which disappeared in the next NWP cycle. O-B monitoring within NWP systems shows promise in identifying anomalies such as these.

3.4. Dependence on atmospheric transmittance

The use by ECMWF and the Met Office of different versions of the FASTEM emissivity model is a large contributor to the differences in O-B PDFs (Figure 10). Since AMSR2 is a microwave imaging instrument, the atmospheric transmittance is high for all its channel frequencies. However, we expect the transmittance to be reduced in regions where the TCWV is high and atmospheric opacity due to water vapour becomes significant. It is interesting, therefore, to explore the interplay between surface emission (determined by FASTEM) and atmospheric absorption and emission (dominated by atmospheric humidity).

Short-range forecasts of TCWV are considered to be well constrained by NWP models. In a typical Met Office NWP global experiment the root mean square (RMS) error in Northern Hemisphere 850 hPa relative humidity at 12 hours forecast range is approximately 15% when verified against radiosondes and 7% when verified against NWP analyses. The respective mean errors are both within 1%. For high TCWV cases the accuracy of the NWP forecast humidity profile will be a major factor determining the spread in O-B.

Figure 13 and Figure 14 illustrate the O-B dependence on the transmittance, which exhibits values below 0.4 at 89 GHz. There is some evidence that the difference between ECMWF and Met Office mean O-Bs for each channel narrows as the transmittance is reduced. A plausible explanation is that, as the sensitivity to the surface is reduced, the two centres' forecast humidity fields act to constrain the departures in a smaller range. Figure 15 illustrates the broad scale agreement of Met Office and ECMWF NWP humidity fields.

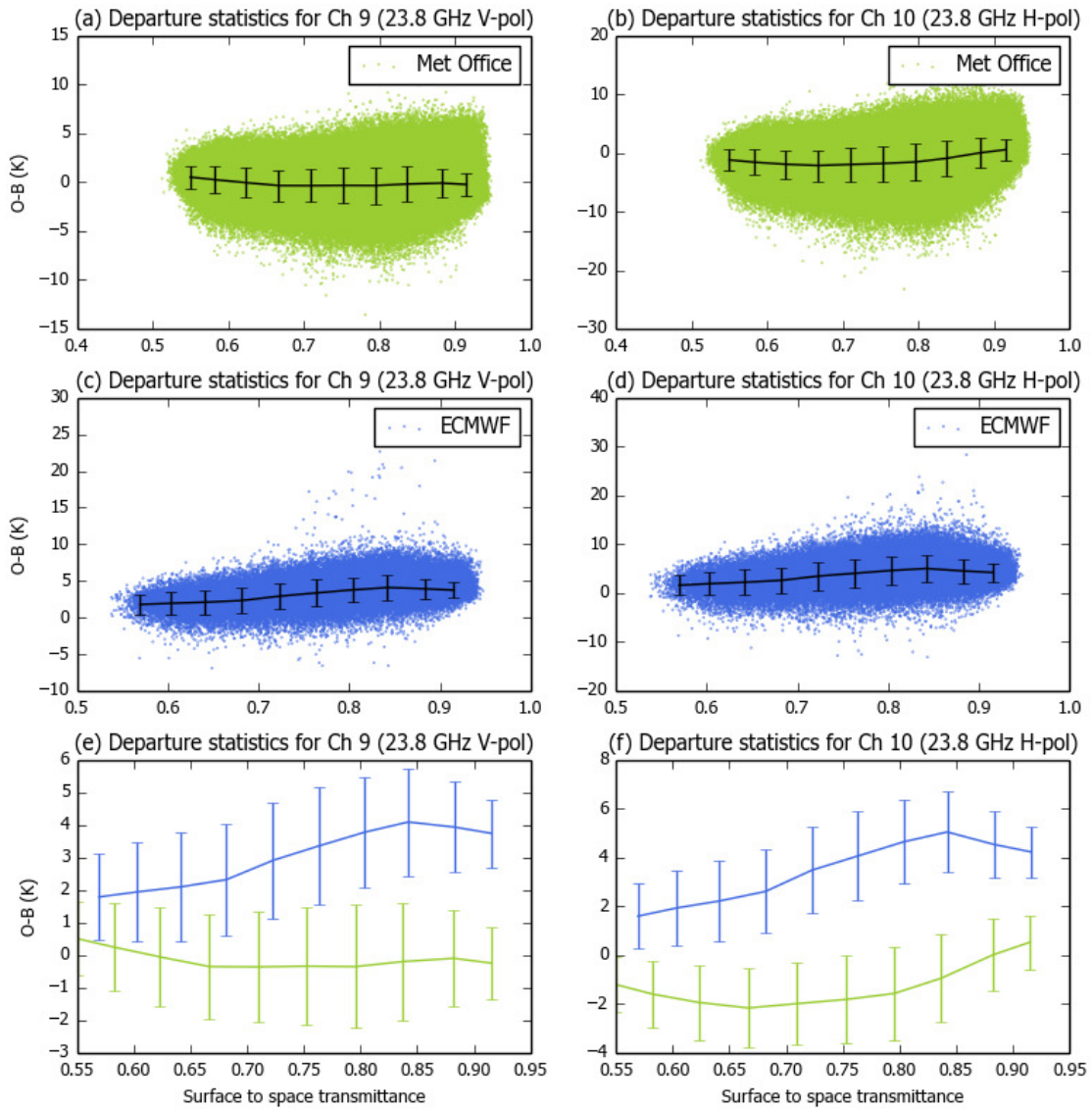


Figure 13. (a) Met Office O-B departures for AMSR2 channel 9 plotted as a function of surface to space transmittance. Each data point is shown as a coloured marker, overlaid with binned data shown in black with error bars. (c) As (a), for ECMWF data. (e) Binned data as in (a) and (c) comparing Met Office and ECMWF statistics. Similarly, departures for AMSR2 channel 10 are shown in (b), (d), (f). Data are shown for May 2015.

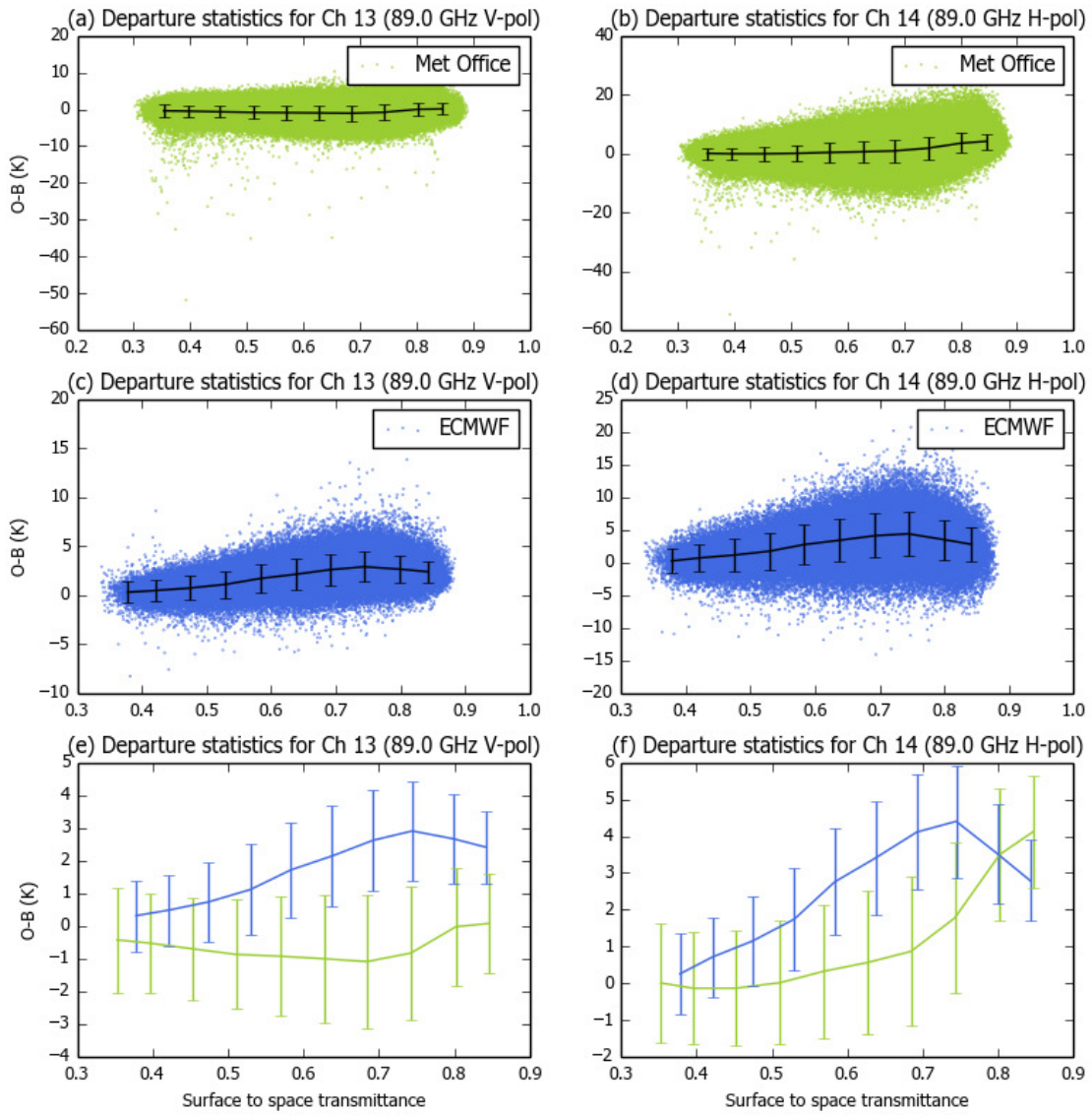


Figure 14. As Figure 13, for AMSR2 channels 13 and 14.

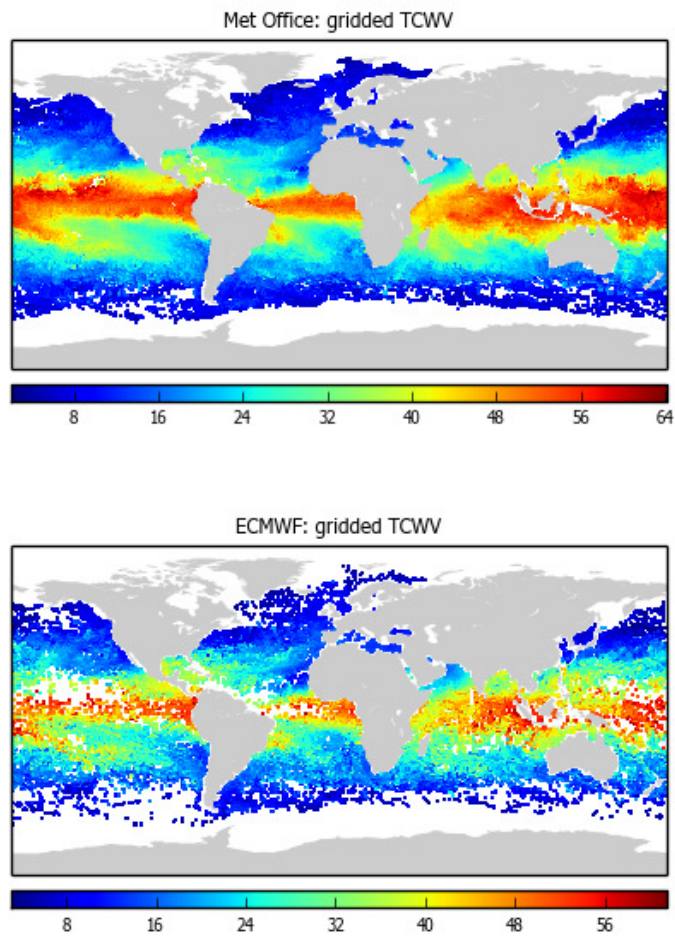


Figure 15. Gridded mean values of total column water vapour in units of kg/m^2 for (top panel) the Met Office data set and (lower panel) ECMWF. Data are shown for April 2015.

3.5. Dependence on orbital angle

Booton et al. (2014) describe the nature of O-B biases for the Special Sensor Microwave Imager Sounder (SSMIS) instruments which have flown on Defense Meteorological Satellite Program (DMSP) satellites. Like AMSR2, SSMIS is a conical scanning radiometer. Booton et al. explain ascending and descending node difference due to calibration anomalies that result from reflector emissivity characteristics and warm load solar intrusions. They develop a bias predictor model to correct the residual bias, as shown in the example in Figure 16.

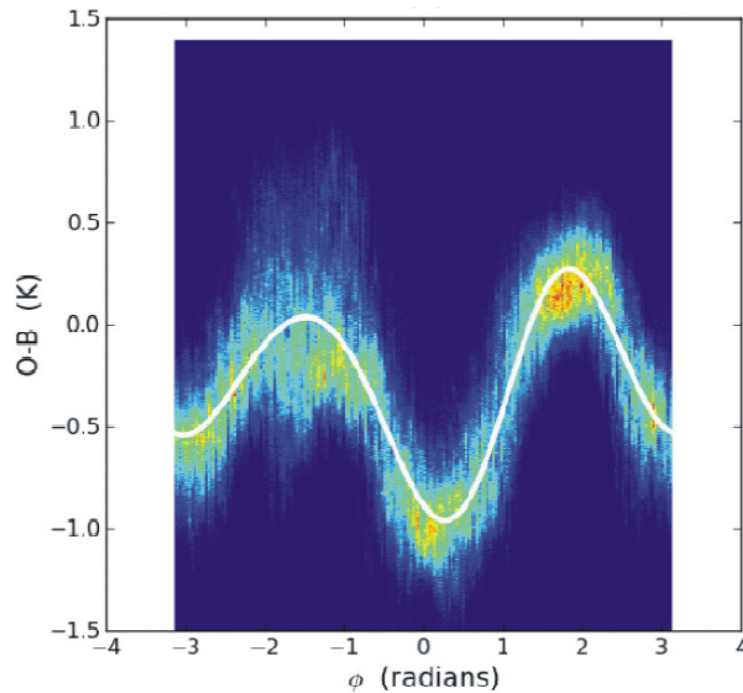


Figure 16. Detail from Fig. 4 in Booton et al. (2014). Two-dimensional histogram of F-18 SSMIS channel 6 O-B. The white line shows the fitted bias as a function of orbital angle ϕ .

Booton et al. define an orbital angle of the satellite's path which is the angle made about the orbital track with respect to the ecliptic plane. The satellite's ascending node intersects the plane at 0° orbital angle. As Figure 16 shows, the variation in O-B around the orbit for SSMIS can be considerable.

The AMSR2 instrument was designed to mitigate against such severe calibration problems. We can see the magnitude of AMSR2 O-B variations as a function of orbital angle⁴ in Figure 17 and Figure 18. Generally, the residual biases seem not to vary markedly around the orbit.

⁴ Booton et al. (2014) make use of the spacecraft position vector to calculate the orbital angle exactly. A slightly simplified calculation is performed here based on footprint coordinates rather than spacecraft coordinates.

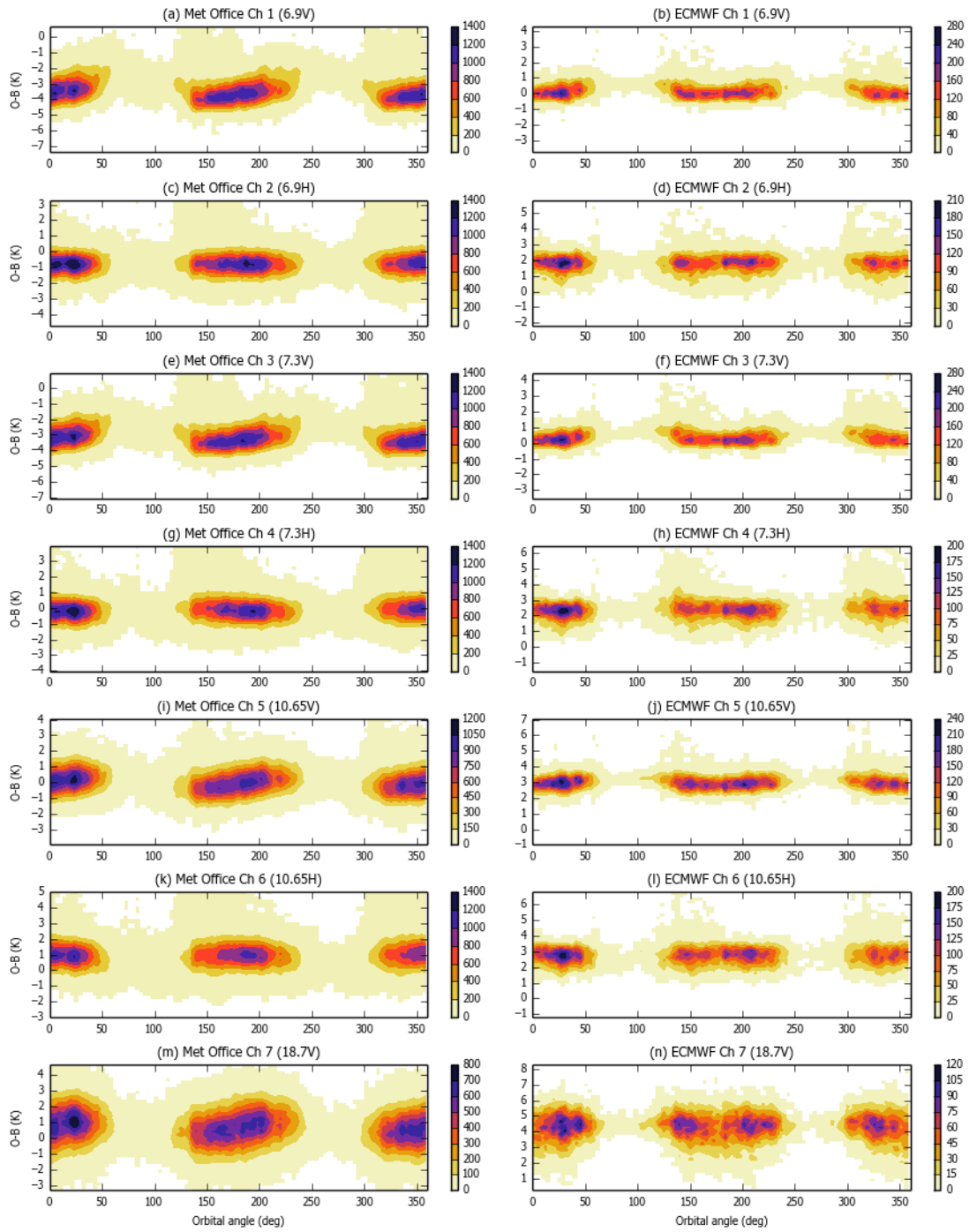


Figure 17. (a), (c), (e), (g), (i), (k), (m) Met Office O-B biases as a function of orbital angle for AMSR2 channels 1-7. Plot contours represent population per two dimensional bin (bin sizes are 3.6° orbital angle and 0.2 K O-B); (b), (d), (f), (h), (j), (l), (n) show ECMWF O-Bs similarly. Data are shown for May 2015.

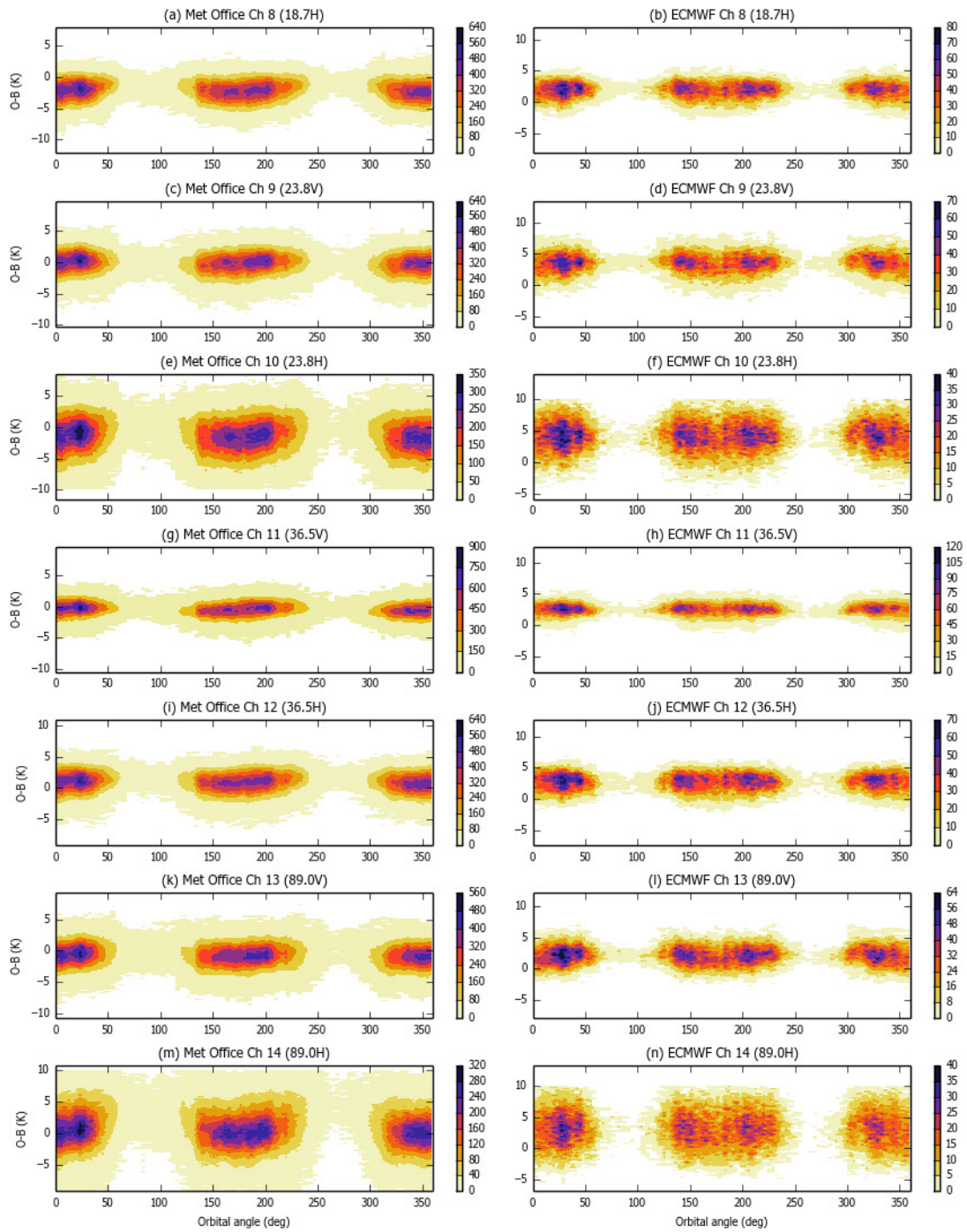


Figure 18. As Figure 17, for AMSR2 channels 8-14.

3.6. Comparison of ascending and descending nodes

The GCOM-W1 spacecraft orbits the Earth in a nearly sun-synchronous path such that the daytime observation is carried out as the satellite traverses with increasing latitude (ascending node) and the night-time observation with decreasing latitude (descending node). We can compare ascending and descending O-B statistics, as shown in the example in Figure 19. For ascending data there is a positive bias that seems to be related to scan position, with largest O-Bs shown in red in Figure 19 (a) and (c). By contrast, for descending data the O-B maps are relatively homogeneous.

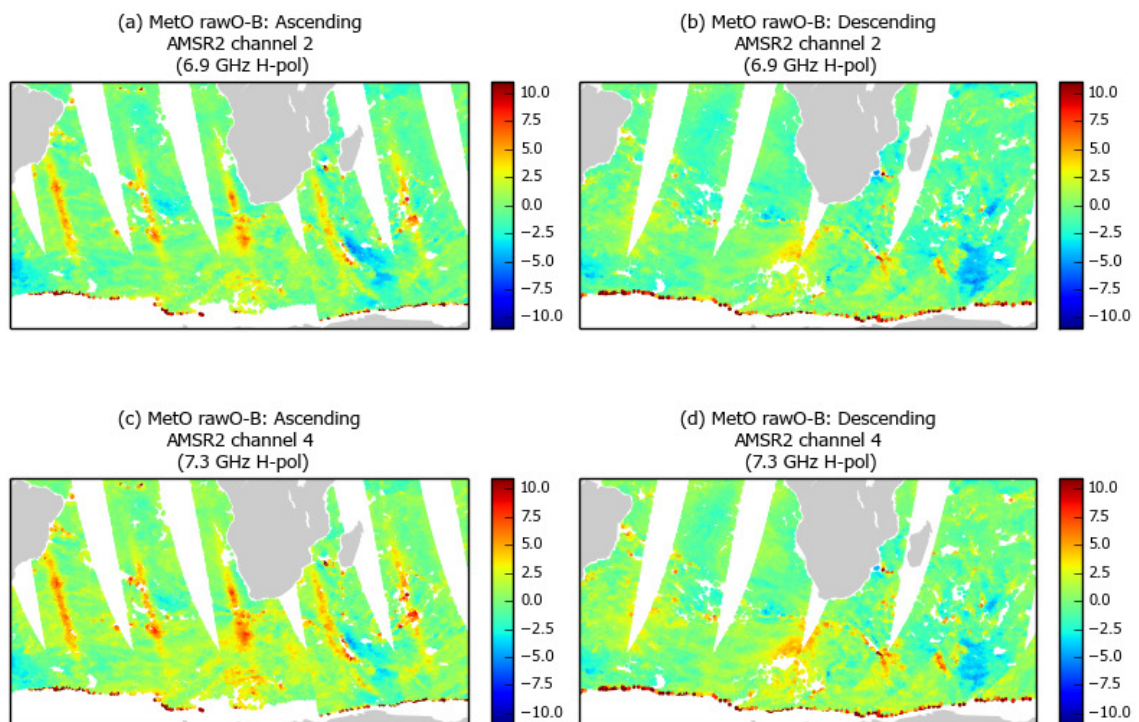


Figure 19. (a) Met Office O-B for AMSR2 channel 2 for ascending node data on 1 May 2015. All data including cloudy observations are shown for a portion of the Southern Hemisphere. (b) As (a), showing the descending node. (c), (d) As (a), (b) for AMSR2 channel 4.

The pattern of biases for the low frequency AMSR2 channels is suggestive of sun glint affecting parts of the daytime orbit. Such effects have been noted previously for AMSR2 (Jones et al., 2015).

3.7. Dependence on scan position

The AMSR2 conical scan provides 243 view positions per revolution with a fixed incidence angle at the Earth's surface. The variation of O-Bs with scan position is shown for the lower frequency channels in Figure 20. Given the contamination of some scenes by sun glint (previous section), these results are partitioned by ascending and descending node. The sun glint appears as a feature in the ascending data near scan position 160 for the lower frequency AMSR2 channels in both centres' data (note that the nominal scan position for ECMWF superobbed data is an average value). At higher frequencies (Figure 21) the O-B dependence on scan position is much less marked. NWP-derived departures are shown to be sensitive to artefacts affecting AMSR2 data quality such as sun glint and RFI.

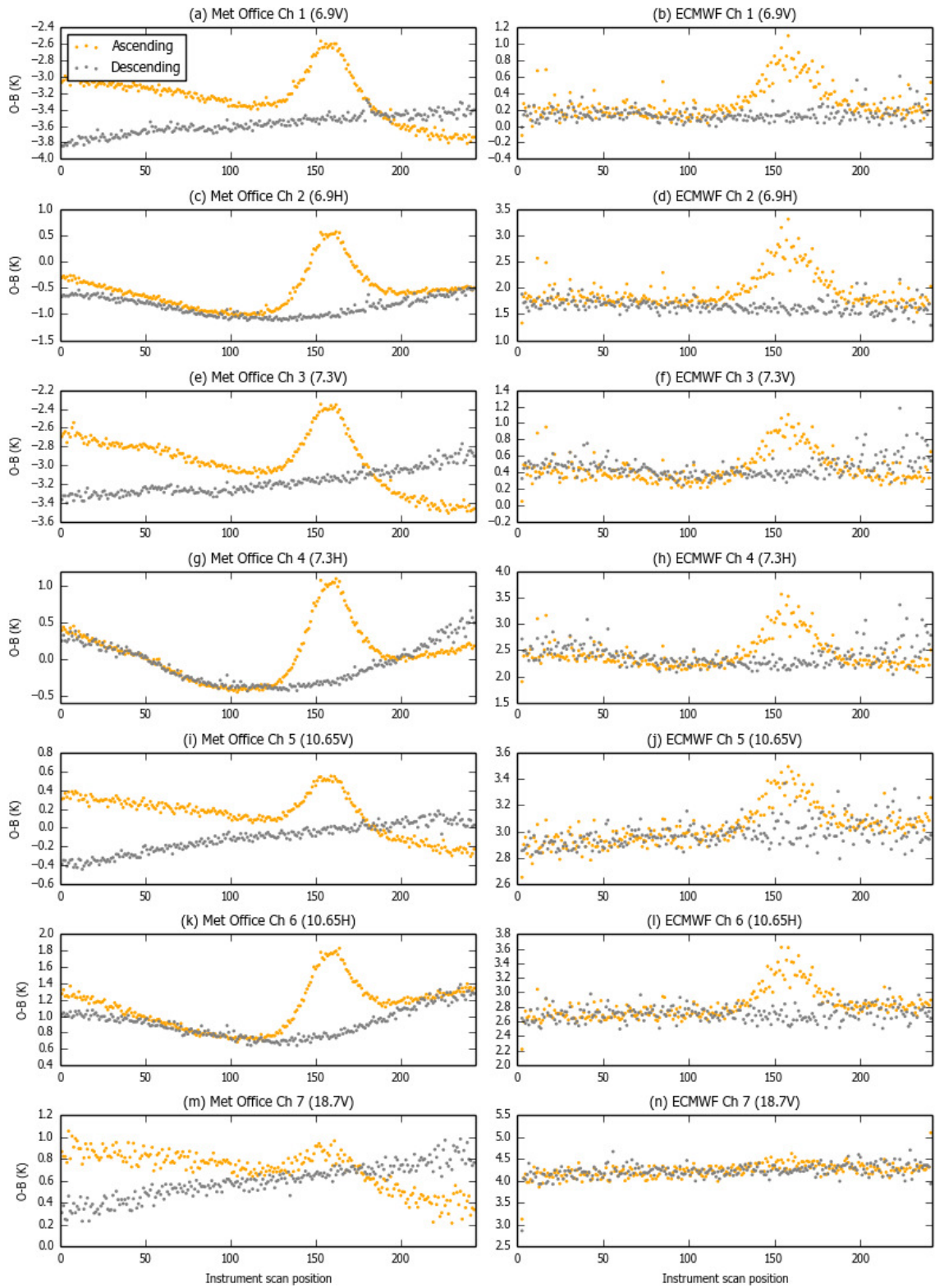


Figure 20. (a), (c), (e), (g), (i), (k), (m) Met Office O-B biases as a function of AMSR2 scan position for channels 1-7; (b), (d), (f), (h), (j), (l), (n) show ECMWF O-Bs similarly. Data are shown for May 2015, separately for ascending node (in orange) and descending node (in grey).

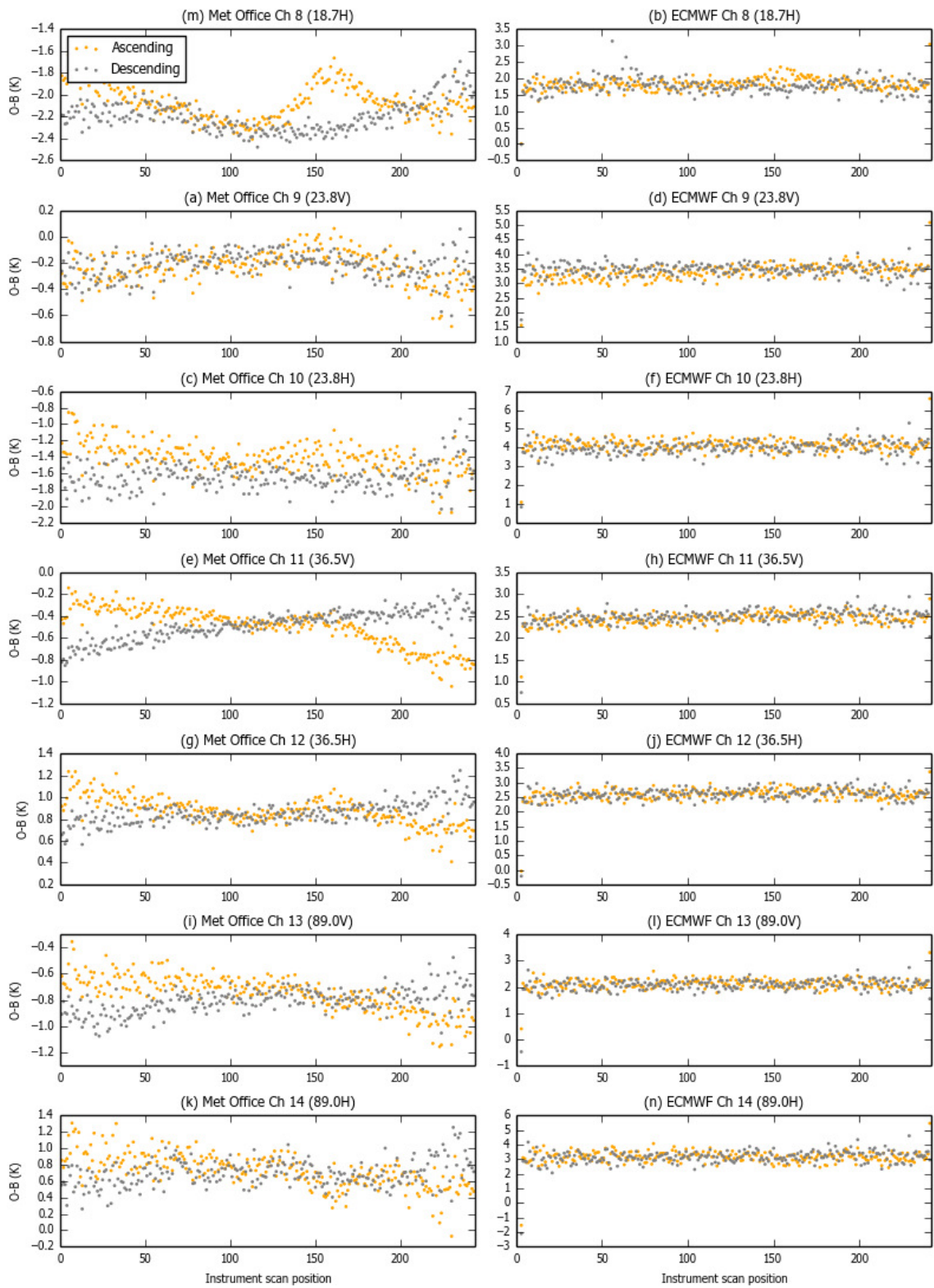


Figure 21. As Figure 20, for AMSR2 channels 8-14.

3.8. Dependence on sea surface temperature

As described previously, all data with SSTs below 275 K have been removed from the data analysis for reasons of quality control. Any remaining influence of SST on the O-Bs may be due to modelled surface emissivity (FASTEM is temperature dependent). Figure 22 and Figure 23 show examples of how the O-Bs vary with SST. Over the range of SSTs sampled, the O-B variation in the binned data is up to 1 K for some channels. It can be seen as a factor in the latitudinal dependence of the O-Bs for some channels seen in the climatology maps, see e.g. Figure 6.

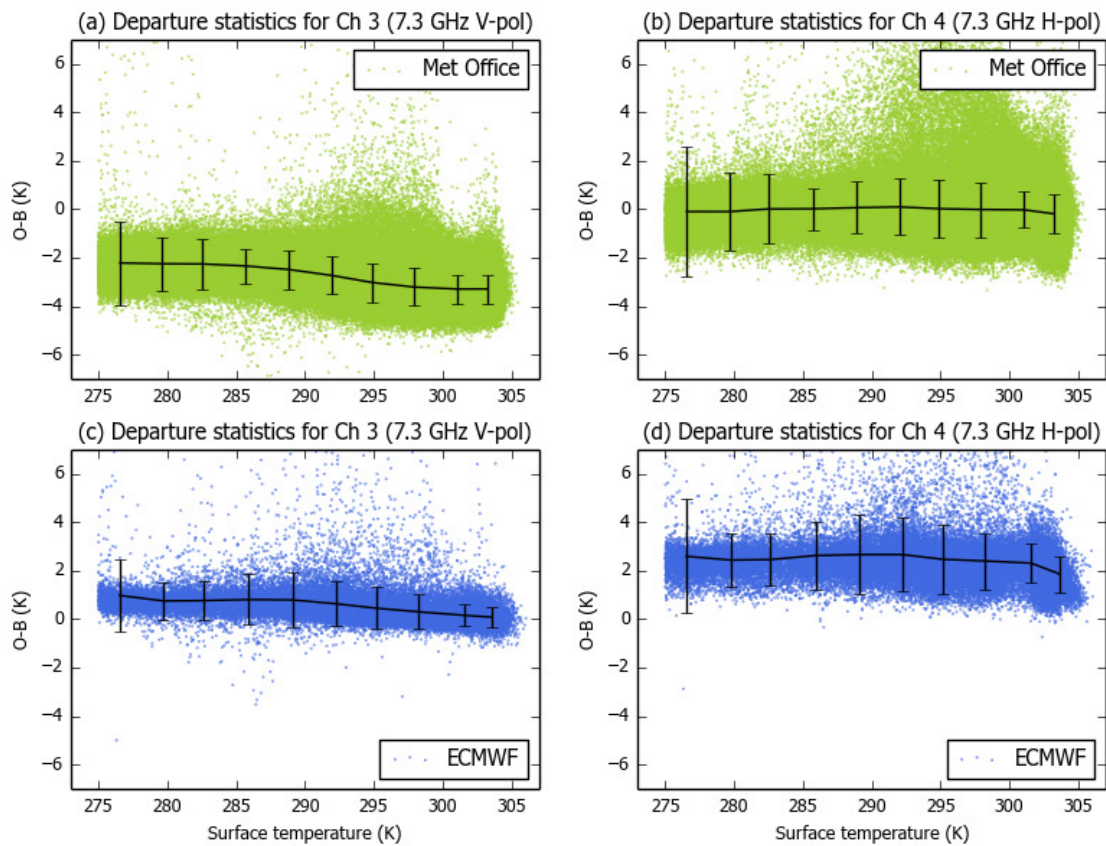


Figure 22. (a) Met Office O-B departure statistics for AMSR2 channel 3 plotted as a function of surface temperature. Each data point is shown as a coloured marker, overlaid with binned data shown in black with error bars. (b) As for (a), showing AMSR2 channel 4 data. (c), (d) As for (a), (b), showing ECMWF data for AMSR2 channels 3 and 4. Data are shown for May 2015.

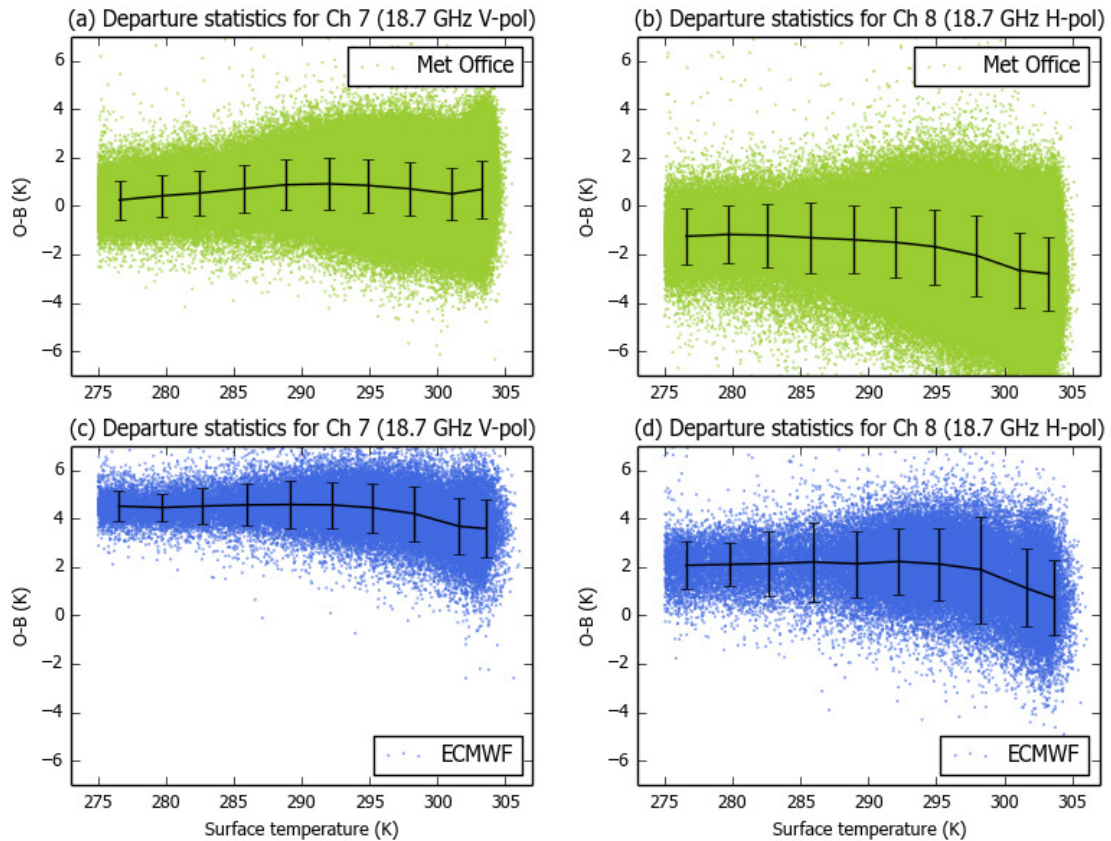


Figure 23. As Figure 22, presenting O-B climatology for AMSR2 channels 7 and 8.

3.9. Daily statistics (seasonal variability)

For evaluation of the quality of ECVs and climate trends derived from satellite data it is important to establish the long-term stability of the instrument calibration as well as the absolute uncertainty in the measurement. The monitoring of O-B statistics in an NWP framework should be well suited for this purpose, since global and temporal coverage is comprehensive and NWP forecast fields are constrained by a large number of conventional and satellite data from numerous sources.

Figure 24 and Figure 25 show daily mean AMSR2 departures for the first six months of the Met Office and ECMWF comparison period (March-August 2015). There are few pronounced trends in the data. For cases where a linear fit produces a gradient of more than 0.1-0.2 K/year, e.g. channel 8 for Met Office data in Figure 25 (a), the corresponding data for the other NWP centre (e.g. ECMWF data in Figure 25 (b)) do not offer corroboration. The advantage of comparing Met Office and ECMWF statistics is that such trends can be cross-checked. The final Year 1 report will contain data for a

longer period which should allow any long-term drifts or effects of the seasonal cycle to be assessed with more confidence.

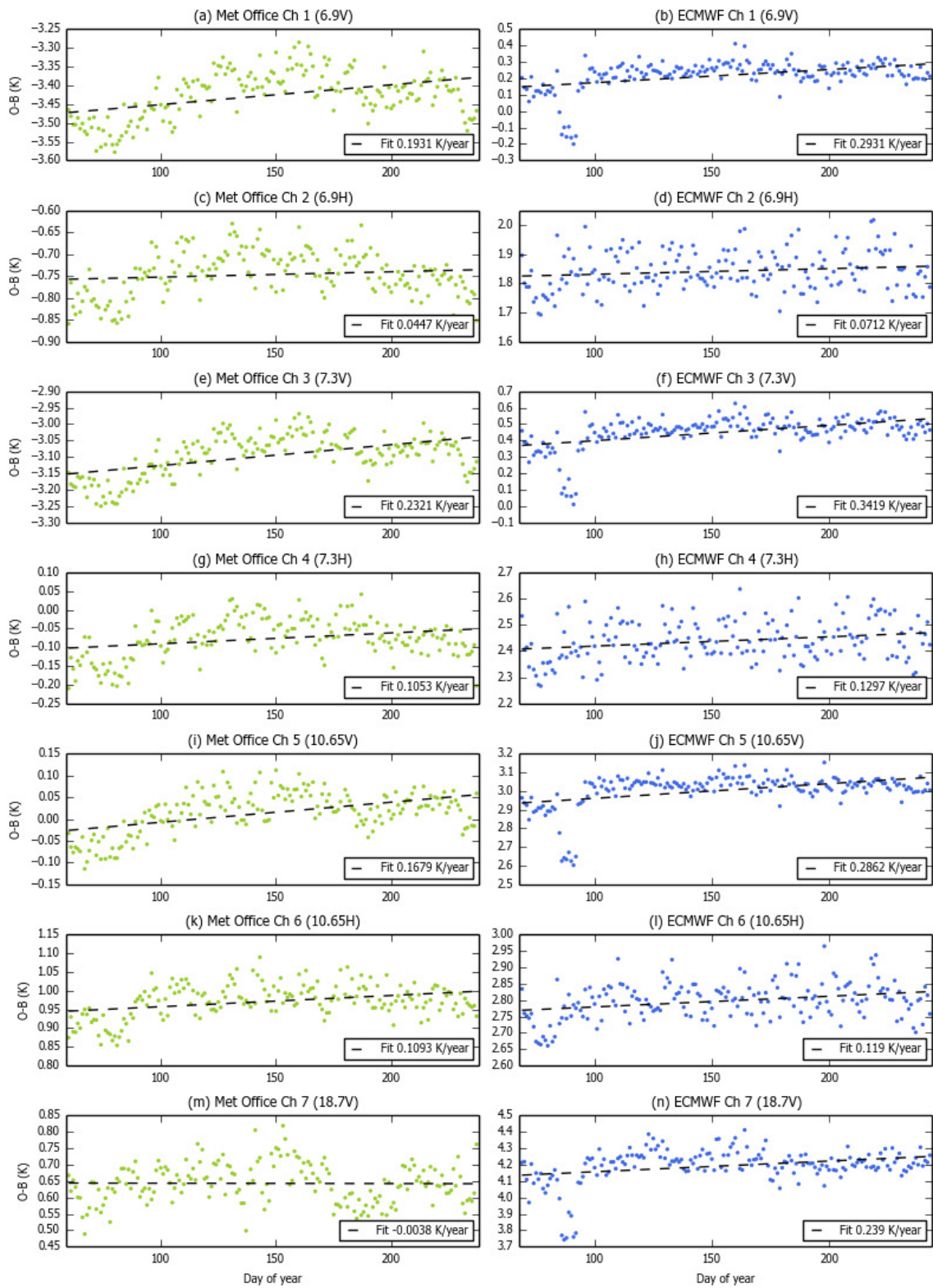


Figure 24. (a), (c), (e), (g), (i), (k), (m) daily mean Met Office O-B as a function of days since 1 January 2015 for channels 1-7; (b), (d), (f), (h), (j), (l), (n) show ECMWF mean O-Bs similarly. The dashed line in each plot is a linear fit to the data with fitted slope recorded in the legend.

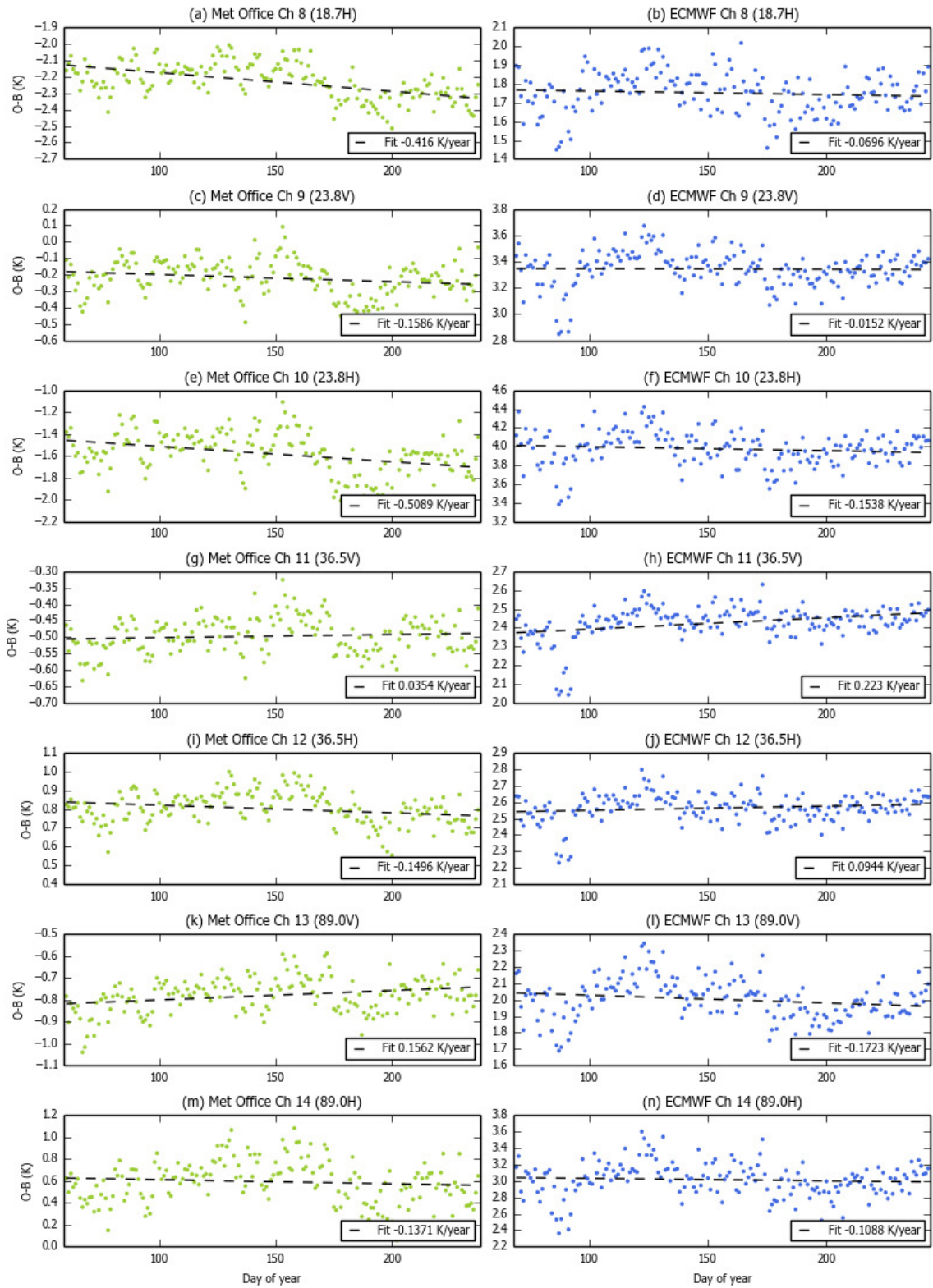


Figure 25. As Figure 24, presenting daily mean O-Bs for AMSR2 channels 8-14.

4. Preliminary conclusions

This report explores the potential for characterisation of satellite instrument performance through the analysis of brightness temperature departures (observed minus background differences) within an NWP framework. As the first of several new satellite missions to be considered for GAIA-CLIM, we investigate the instrument data quality for AMSR2. We have analysed quality-controlled data sets derived from state-of-the-art DA systems and forecast models developed independently by ECMWF and the Met Office. Scenes that are difficult to model well or are subject to radiative transfer errors, such as areas of cloud or high winds, have been excluded from the final data.

PDFs of the departures (Figure 10) reveal inconsistencies between the Met Office and ECMWF statistics, whereby the mean ECMWF O-B for each AMSR2 channel is consistently higher. The main driver for the difference is shown to be the model used to generate ocean emissivity estimates as input to the radiative transfer calculations: ECMWF uses FASTEM-6 which predicts a lower emissivity than the FASTEM-3 model used at the Met Office. This study exposes the need for reduced uncertainties in model ocean emissivity over the 6-90 GHz range in order to make full use of microwave imager radiances and ECVs derived from the observations.

An imperfect knowledge of the surface emissivity is a barrier to quantifying, through analysis of O-B statistics, robust uncertainty estimates for individual AMSR2 channels. However, we show (Figure 13) a narrowing of the discrepancy between Met Office and ECMWF mean O-B for scenes where the atmospheric transmittance is lower, sensitivity to the surface is correspondingly reduced, and simulated radiances are more sensitive to model representations of the global humidity field.

Some localised incidences of large departures have been identified and attributed to RFI contamination and sun glint. NWP monitoring of O-B statistics, given its comprehensive coverage, is shown to be of use in making these identifications. Similarly, by investigating how the mean biases vary around the satellite orbit (Figure 17, Figure 18) we can exclude for AMSR2 the kind of serious orbit-related calibration instabilities seen previously for SSMIS.

It is important to monitor long-term drifts in satellite radiances to ensure the robustness of ECV trends derived from the data. The stability of NWP fields used for this purpose, when compared with reference-quality observations, is a prerequisite that will be

addressed during GAIA-CLIM. This report contains a preliminary investigation of AMSR2 calibration stability (Figure 24 and Figure 25). As we extend the time period considered, the confidence in the magnitude of long-term drifts will be improved.

5. Acknowledgements

This project has received funding from the European Union's Horizon 2020 research and innovation programme under grant agreement No 640276. We thank colleagues at the Met Office (Stefano Migliorini and Fabien Carminati) and ECMWF (Steve English, Bruce Ingleby, Peter Lean and Alan Geer) for their assistance and useful discussions during the project.

6. References

- Auligné, T., A. P. McNally and D. P. Dee, Adaptive bias correction for satellite data in a numerical weather prediction system. *Q. J. Royal Met. Soc.*, **133**, 631–642 (2007).
- Booton, A., W. Bell and N. Atkinson, An improved bias correction for SSMIS, *Proceedings of the 19th International TOVS Study Conference (ITSC-19)*, Jeju Island, South Korea (2014).
http://cimss.ssec.wisc.edu/itwg/itsc/itsc19/program/papers/10_03_booton.pdf
- Geer, A. J., and P. Bauer, Observation errors in all-sky data assimilation. *Q. J. Royal Meteorol. Soc.*, **137**, 2024–2037 (2011).
- Geer, A. J., F. Baordo, N. Bormann and S. English, All-sky assimilation of microwave humidity sounders, *ECMWF Technical Memorandum No. 741* (2014).
<http://www.ecmwf.int/sites/default/files/elibrary/2014/9507-all-sky-assimilation-microwave-humidity-sounders.pdf>
- Imaoka, K., M. Kachi, M. Kasahara, N. Ito, K. Nakagawa and T. Oki, Instrument performance and calibration of AMSR-E and AMSR2, *International Archives of the Photogrammetry, Remote Sensing and Spatial Information Science*, Volume XXXVIII, Part 8, Kyoto Japan (2010).
http://www.isprs.org/proceedings/XXXVIII/part8/pdf/JTS13_20100322190615.pdf
- Jones, E., K. Garrett, E. Maddy and S. Boukabara, The Assimilation of AMSR2, GMI, and SAPHIR Data in the NCEP GDAS, presented at 13th JCSDA Technical Review and Science Workshop, May 2015.
http://www.jcsda.noaa.gov/documents/meetings/wkshp2015/posters/EJones_JCSDAawks_hp_2015.pdf
- Kazumori, M. and S.J. English, Use of the ocean surface wind direction signal in microwave radiance assimilation. *Q. J. Royal Met. Soc.*, **141**, 1354–1375 (2015).
- Kazumori, M., Geer, A. J. and English, S. J., Effects of all-sky assimilation of GCOM-W/AMSR2 radiances in the ECMWF numerical weather prediction system. *Q. J. Royal Met. Soc.* doi: 10.1002/qj.2669 (2015).
- Liu, Q. and F. Weng, Retrieval of sea surface wind vector from simulated satellite microwave polarimetric measurements. *Radio Sci.* **38**, 8078 (2003). doi: 10.1029/2002RS002729
- Lu, Q. and W. Bell, Characterizing Channel Center Frequencies in AMSU-A and MSU Microwave Sounding Instruments. *J. Atmos. Oceanic Technol.*, **31**, 1713–1732 (2014).
http://www.jcsda.noaa.gov/documents/meetings/wkshp2015/posters/EJones_JCSDAawks_hp_2015.pdf
- Petty, G., Physical retrievals of over-ocean rain rate from multichannel microwave imagery. Part I: Theoretical characteristics of the normalised polarisation and scattering indices. *Meteorol. Atmos. Phys.*, **54**, 79–99 (1994).
- Petty, G., and K. Katsaros, Precipitation observed over the South China Sea by the Nimbus-7 scanning multichannel microwave radiometer during winter MONEX. *J. Appl. Meteorol.*, **29** 273–287 (1990).

Rabier, F., H. Järvinen, E. Klinker, J.-F. Mahfouf and A. Simmons, The ECMWF operational implementation of four-dimensional variational assimilation. I: Experimental results with simplified physics. *Q. J. Royal Meteorol. Soc.*, **126**, 1143-1170 (2000).

Rawlins, F., S. P. Ballard, K. J. Bovis, A. M. Clayton, D. Li, G. W. Inverarity, A. C. Lorenc and T. J. Payne, The Met Office global four-dimensional variational data assimilation scheme. *Q. J. Royal Meteorol. Soc.*, **133**, 347–362 (2007)

Saunders R.W., M. Matricardi and P. Brunel, An Improved Fast Radiative Transfer Model for Assimilation of Satellite Radiance Observations. *Q. J. Royal Meteorol. Soc.*, **125**, 1407-1425 (1999).

7. Appendix: monthly O-B climatology maps

Monthly climatologies of O-B are presented here, summarising the Met Office and ECMWF data sets.

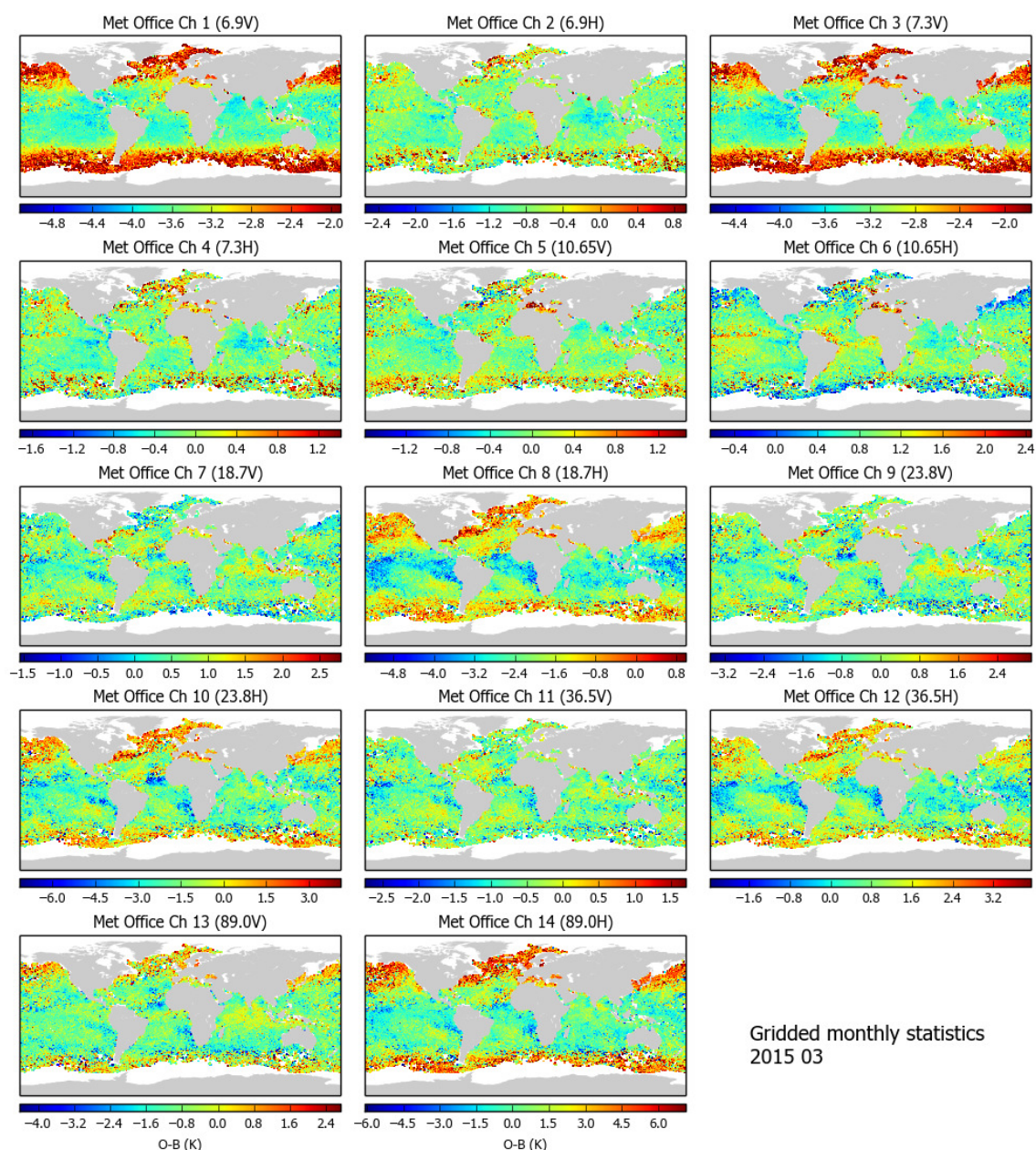


Figure 26. Met Office AMSR2 O-B mean data for March 2015, presented on 1° longitude \times 1° latitude grid. Channels 1-14 are shown as denoted in the headings.

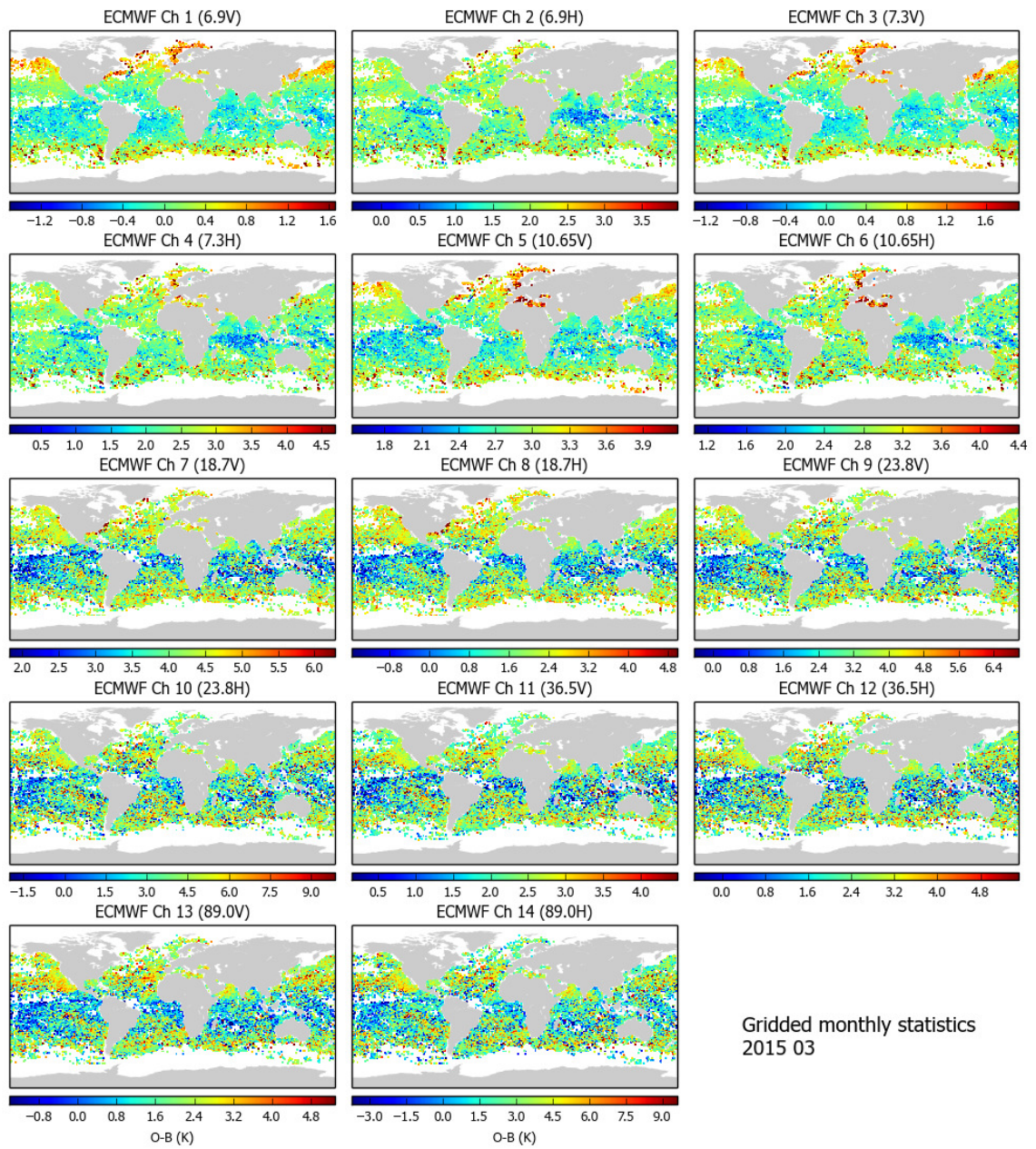


Figure 27. As Figure 26, ECMWF gridded O-B for March 2015.

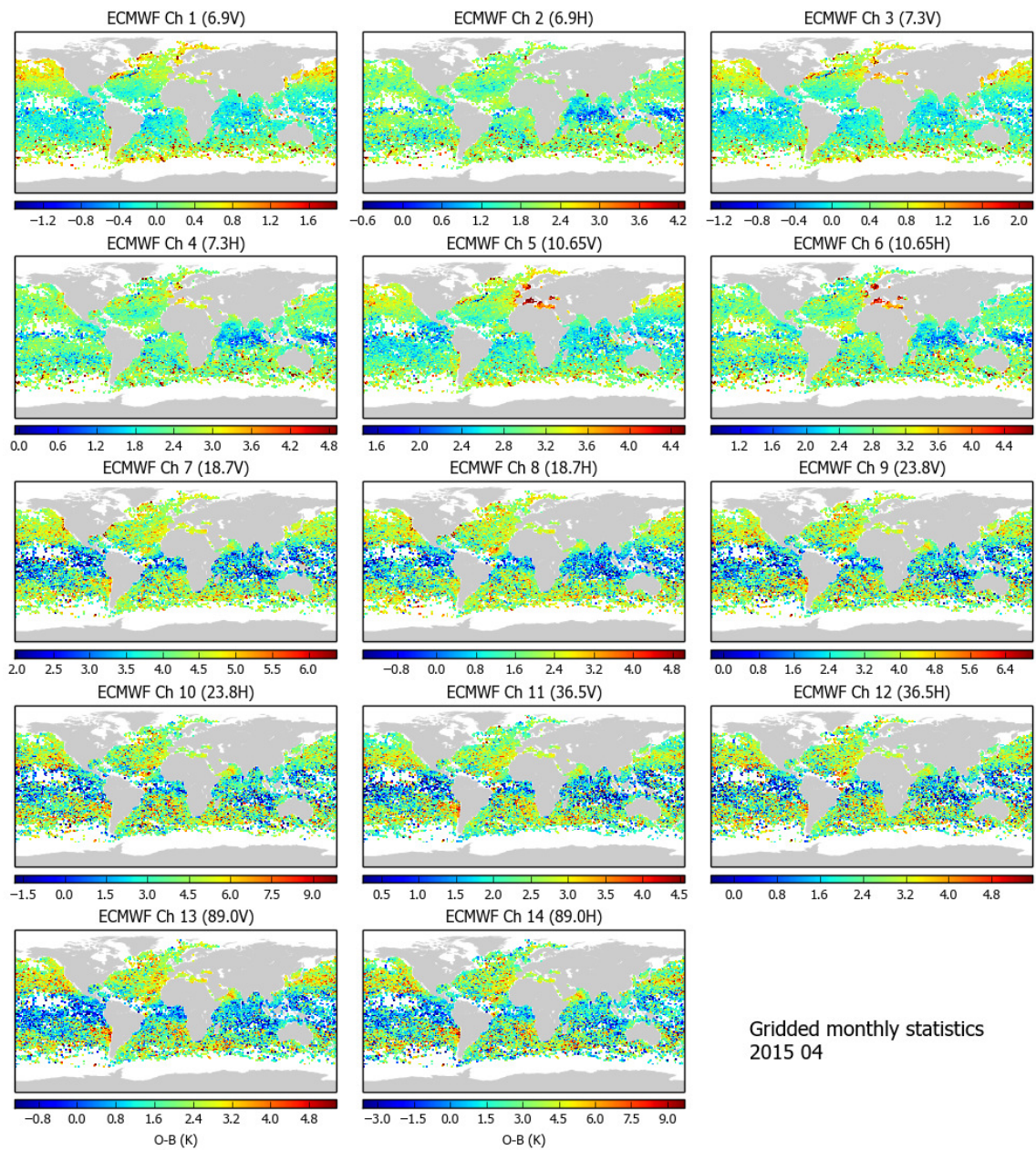


Figure 29. As Figure 26, ECMWF gridded O-B for April 2015.

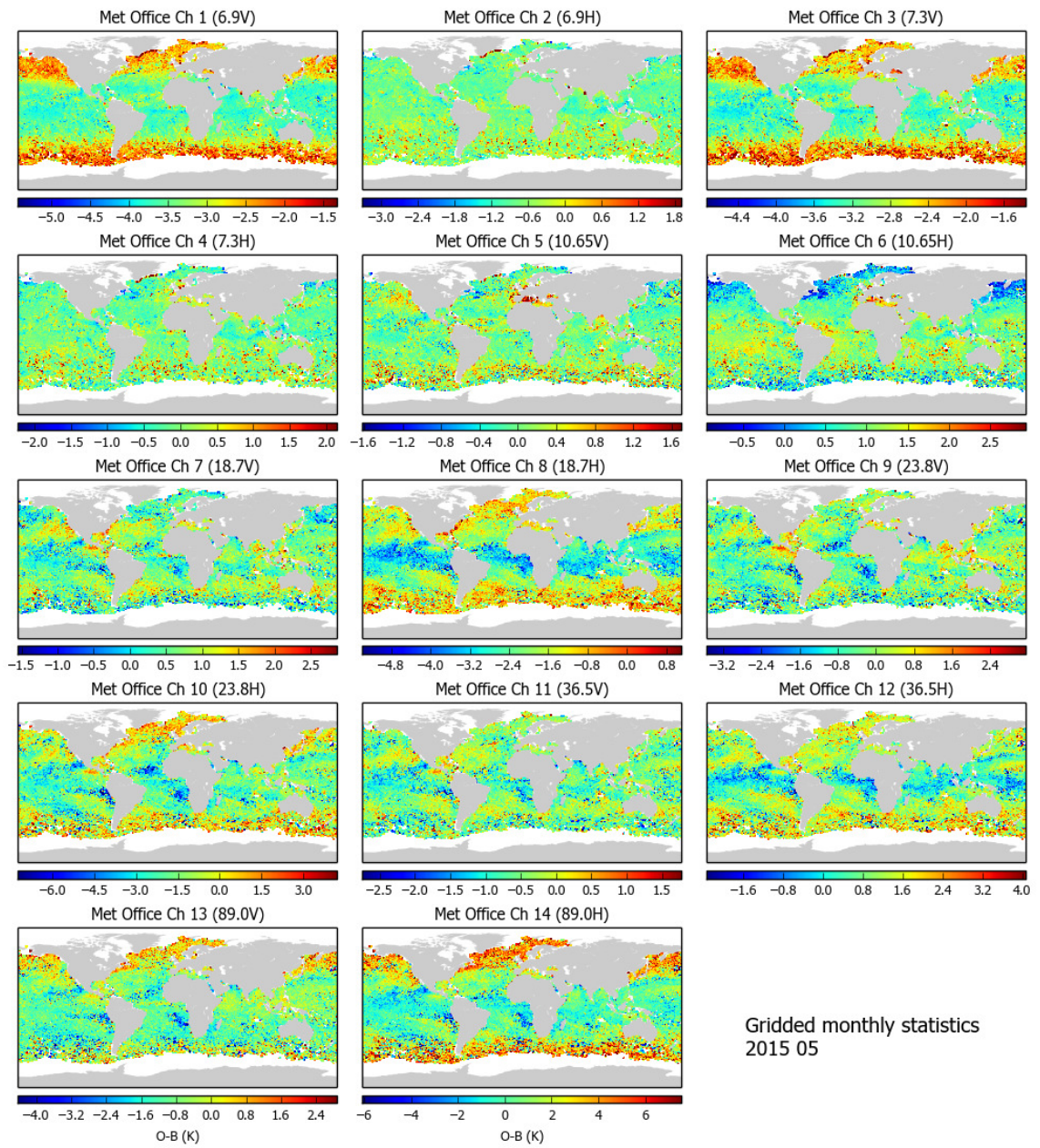


Figure 30. As Figure 26, Met Office gridded O-B for May 2015.

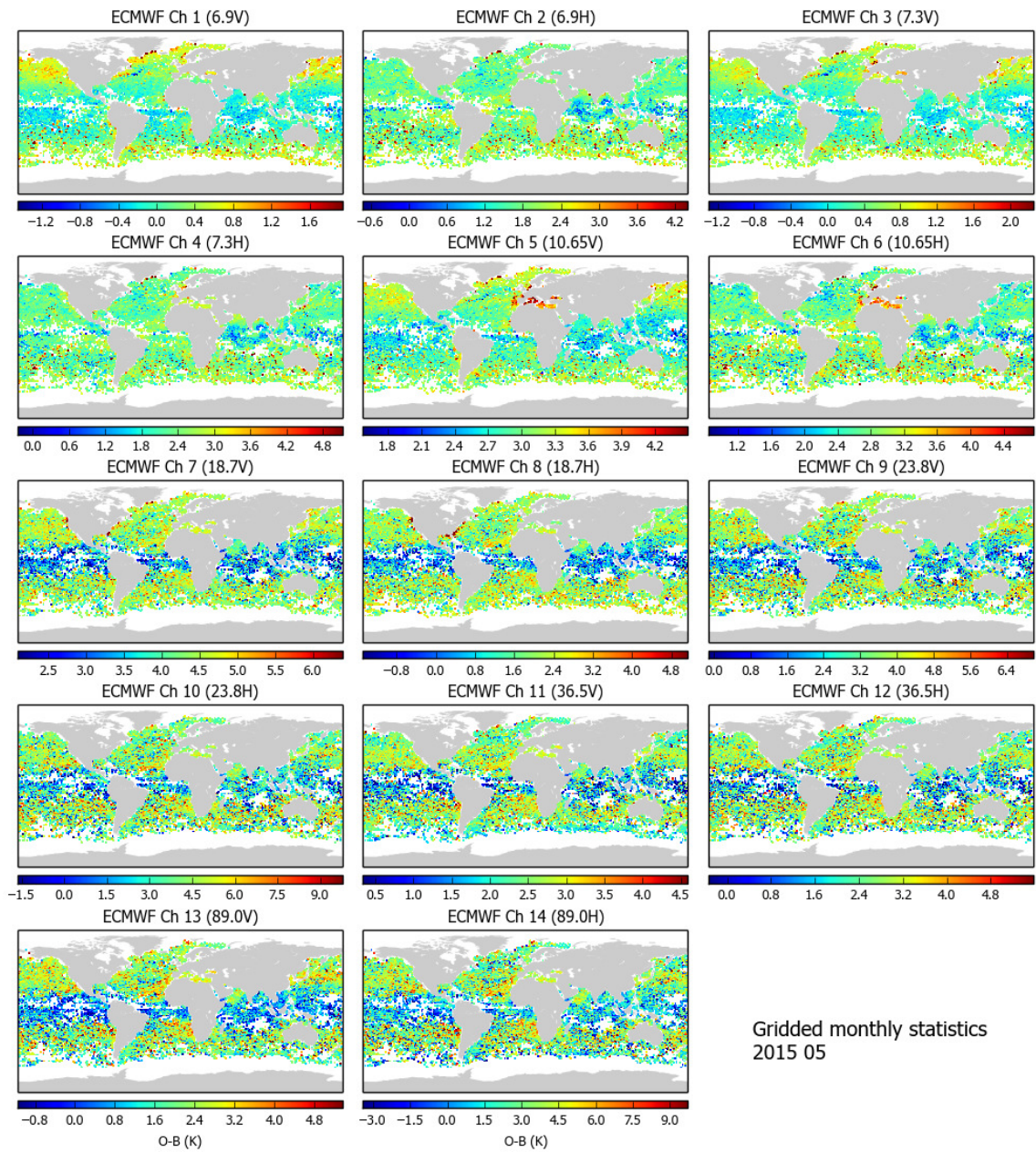


Figure 31. As Figure 26, ECMWF gridded O-B for May 2015.

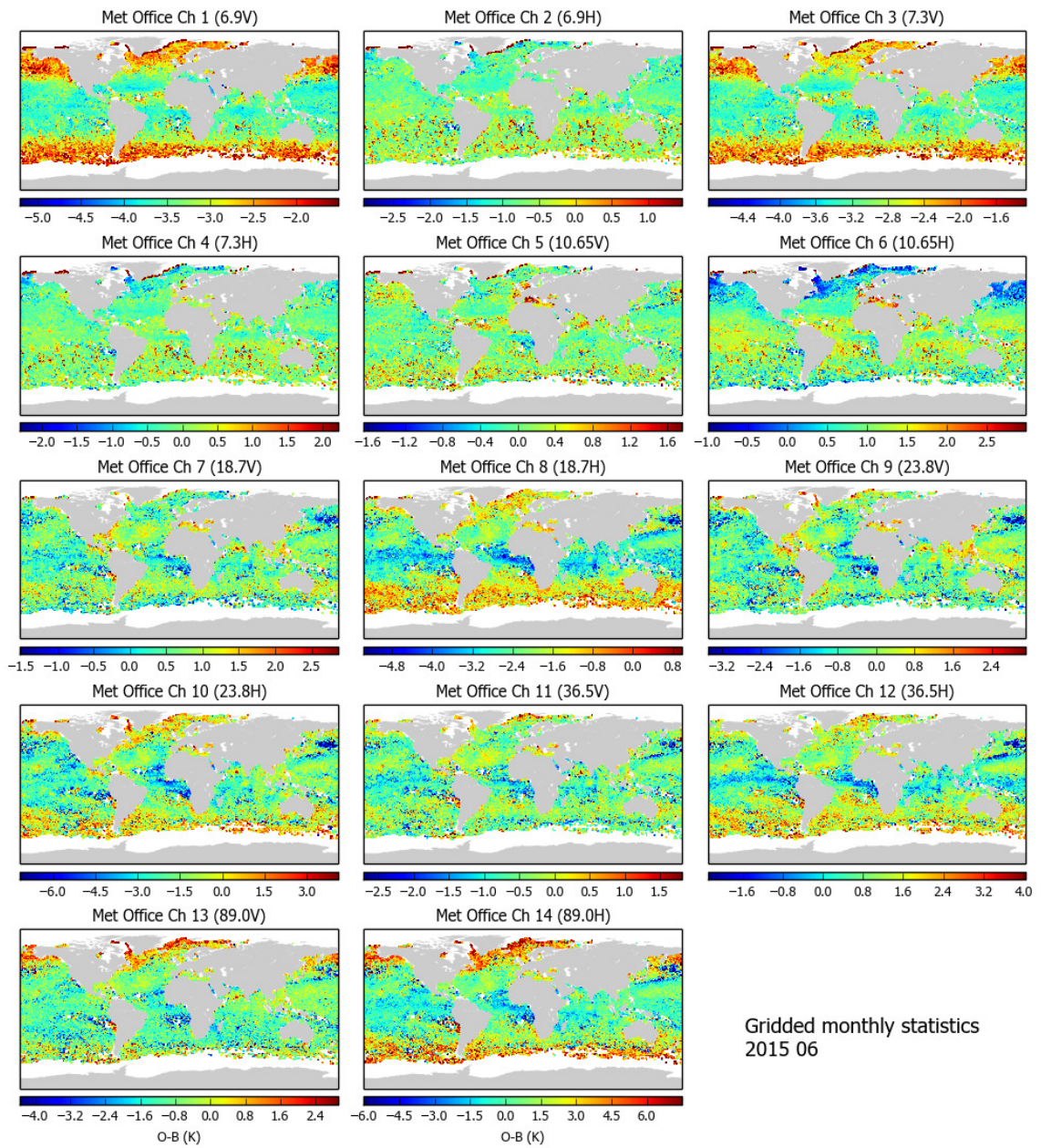


Figure 32. As Figure 26, Met Office gridded O-B for June 2015.

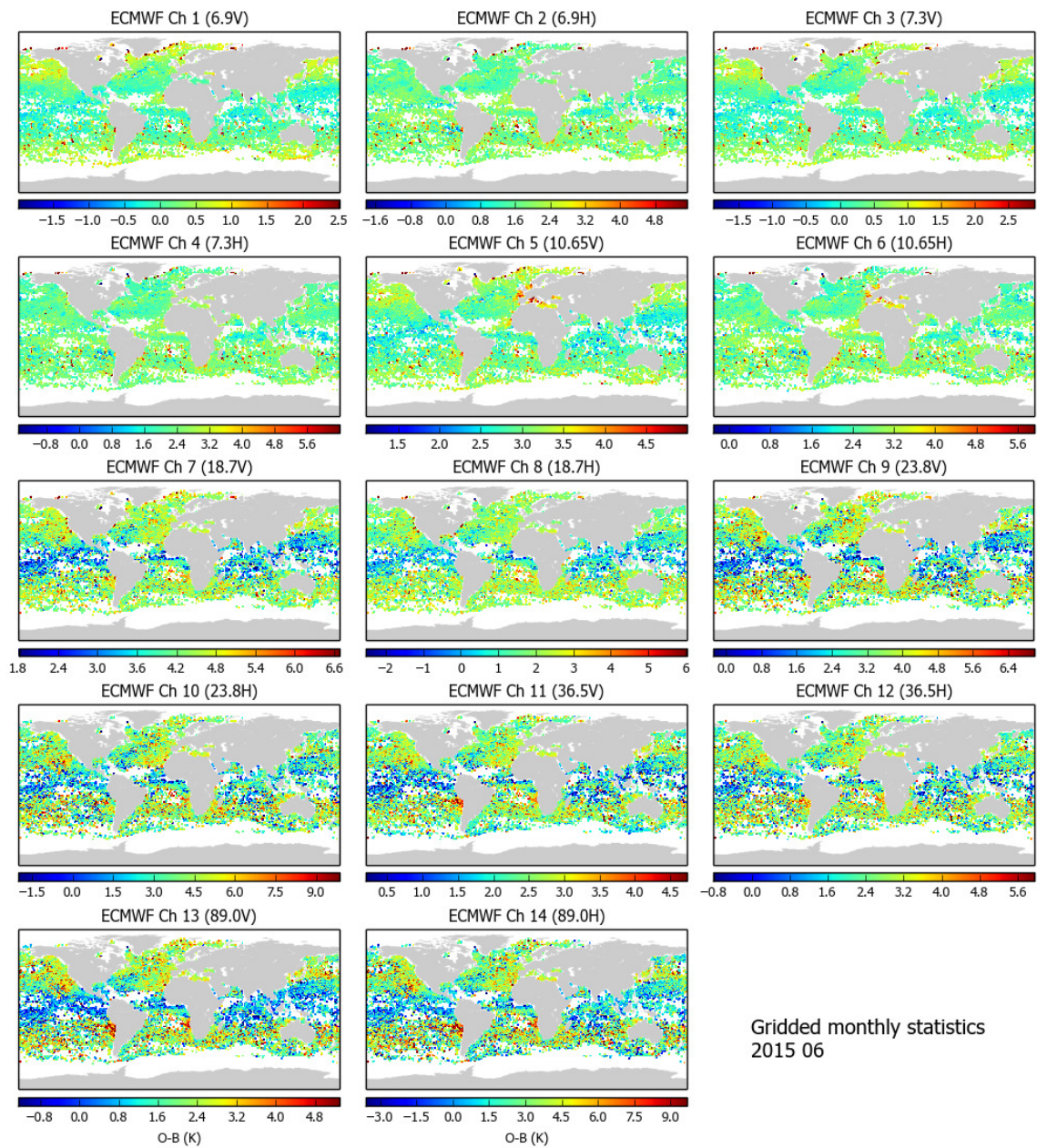
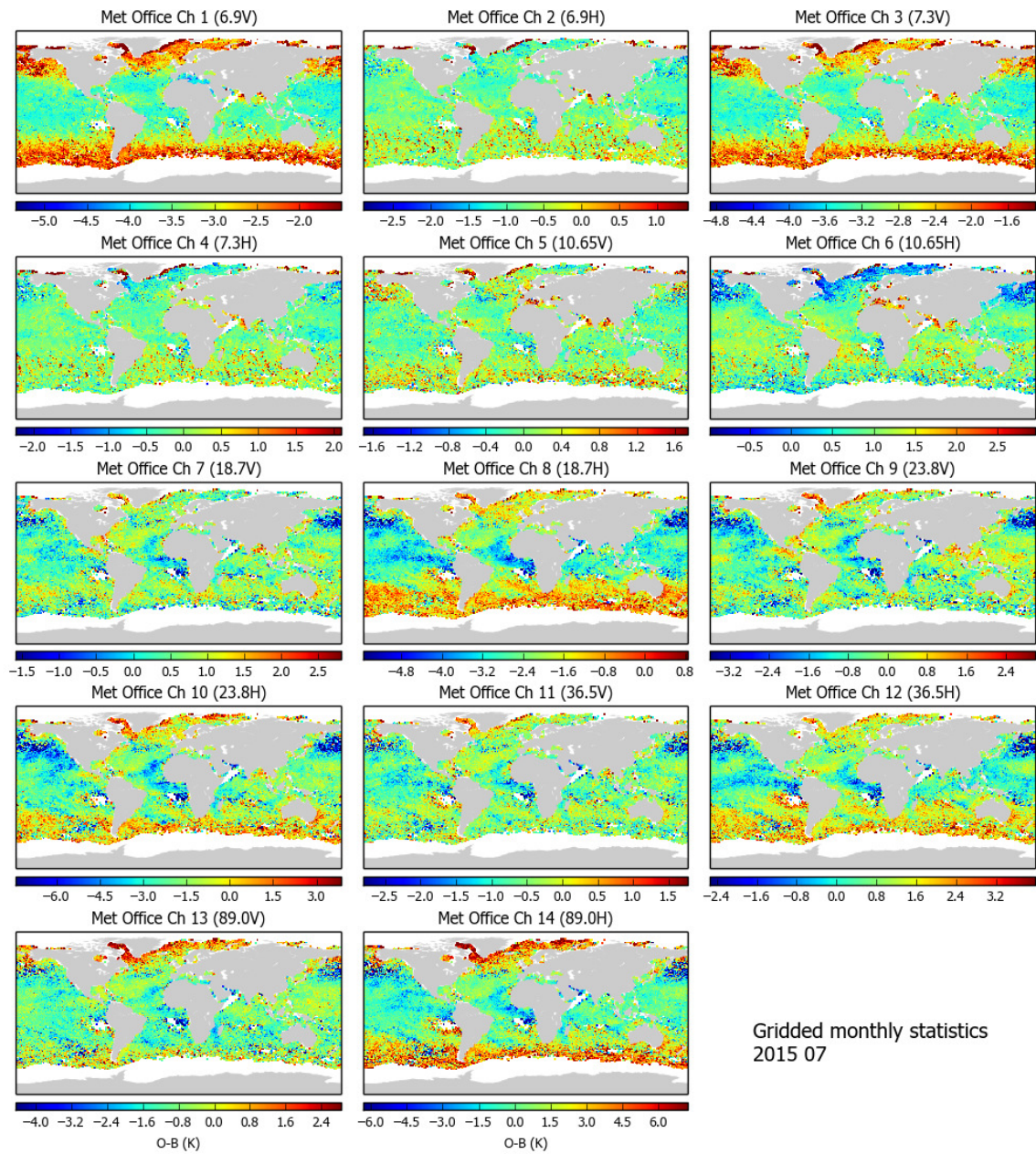


Figure 33. As Figure 26, ECMWF gridded O-B for June 2015.



Gridded monthly statistics
2015 07

Figure 34. As Figure 26, Met Office gridded O-B for July 2015.

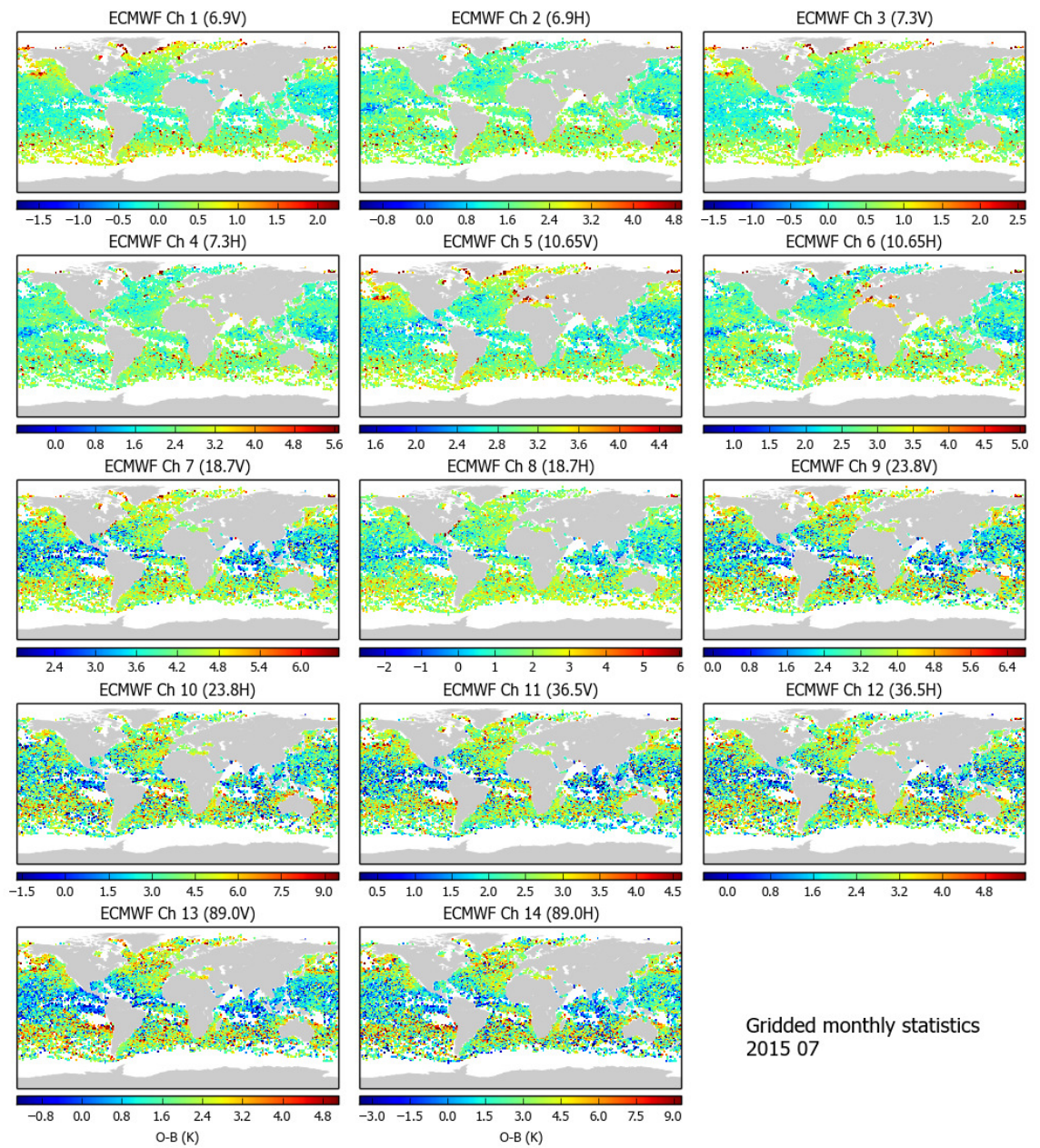


Figure 35. As Figure 26, ECMWF gridded O-B for July 2015.

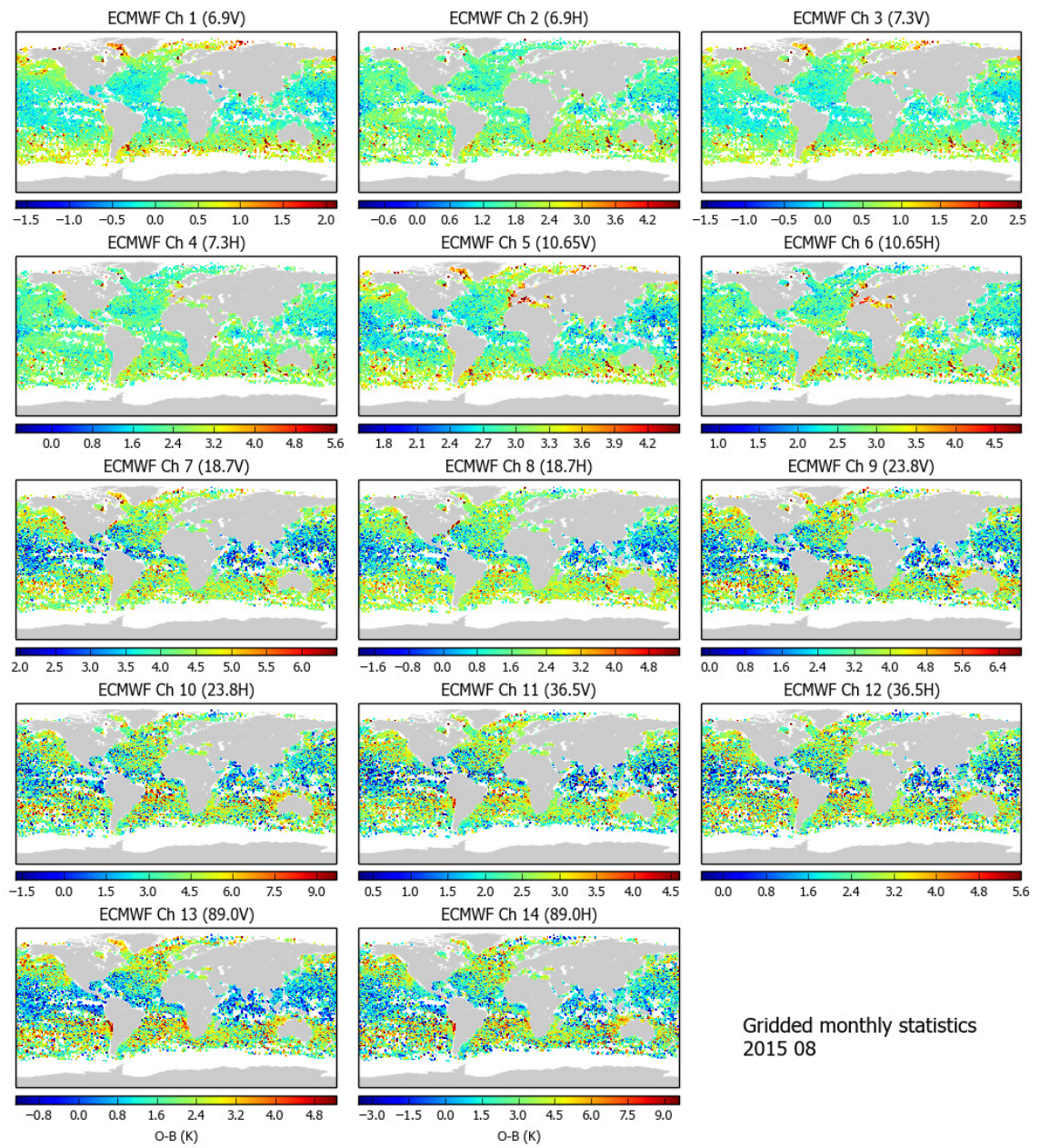


Figure 37. As Figure 26, ECMWF gridded O-B for August 2015.